ANALYTICAL MODELLING OF IMPURITY TRANSPORT IN TOROIDAL DEVICES

G. Fussmann

IPP III/105 August 1985

MAX-PLANCK-INSTITUT FÜR PLASMAPHYSIK

8046 GARCHING BEI MÜNCHEN

MAX-PLANCK-INSTITUT FÜR PLASMAPHYSIK

GARCHING BEI MÜNCHEN

ANALYTICAL MODELLING OF IMPURITY TRANSPORT IN TOROIDAL DEVICES

G. Fussmann

IPP III/105 August 1985

Die nachstehende Arbeit wurde im Rahmen des Vertrages zwischen dem Max-Planck-Institut für Plasmaphysik und der Europäischen Atomgemeinschaft über die Zusammenarbeit auf dem Gebiete der Plasmaphysik durchgeführt.

IPP III/105 G. Fussmann ANALYTICAL MODELLING OF IMPURITY TRANSPORT IN TOROIDAL DEVICES

Abstract

This review deals with our knowledge of the fundamentals of impurity transport in tokamaks and stellarators. Emphasis is put on the processes in the edge region, which are of crucial importance for wall-produced impurities. For the anomalous-transport model closed analytic expressions for the stationary case are derived which allow the importance of various transport and plasma parameters to be estimated. We also discuss some general features of non-stationary problems. In particular, the definitions and essentials of various characteristic times are discussed. Moreover, we elucidate the questions of diffusive penetration and impurity screening.

Contents

1. Introduction

The control of impurities is still one of the salient problems in nuclear fusion devices such as tokamaks and stellarators. Although the impurity concentrations have been reduced to tolerable levels ($Z_{eff} < 2$, $P_{radiation}/P_{input} < 30$ %) in many experiments during the ohmic heating phase by choosing suitable materials or by means of divertors, the impurity problem again appears with additional heating when the power fluxes are considerably increased. The whole impurity complex can be subdivided into production of impurities, first ionization (deposition profiles), and transport of the impurity ions, all three aspects being of equal importance. It is therefore necessary, on the one hand, to know the dominant mechanisms causing the production of a specific impurity, but, on the other, one must also understand the transport of the released particles to estimate the effect on the plasma performance.

This paper deals with the deposition and transport aspect for the purpose of reviewing and discussing the basic ideas of impurity transport currently prevailing. Most of the published theoretical work is devoted to the transport in the inner plasma region with closed magnetic surfaces. However, as outlined in Sec. 2, the actual impurity problem is generally strongly governed by the screening processes in the relatively thin scrape-off region. One of the main objectives of this paper is the derivation of eqs. (18), (25) and (28), which allows us to calculate the impurity density in the inner plasma region for a given stationary influx of neutral atoms. A simplified formula for the same purpose was first obtained by Engelhardt and Feneberg /1/, who assumed an anomalous diffusion coefficient $D_\perp$ and imposed a hard-boundary condition by setting the impurity ion density n^+ equal to zero at the limiter edge. It was further assumed that the neutrals are effectively ionized within a distance λ_i from the edge. The relation they obtained, $n^+(r=o) = \Gamma_o \lambda_i/D$, already shows the combined influence of transport ($D_\perp$) and deposition in the boundary region (λ_i). A considerable improvement of the above formula was presented by Engelhardt et al. in Ref. /2/, where, in particular, the hard-boundary condition was replaced by a loss term in the scrape-off layer (soft boundary). On the other hand, this treatment also included some unrealistic idealizations (linear geometry, n_e = const.). Recently Lackner et al. /3/ derived an expression which is identical with our eq. (18) for the case $D_\perp$ = const. and $v_\perp = 0$. However, a finite drift velocity $v_\perp$ - for which experimental evidence has been found under certain plasma conditions /4/ - can have a drastic impact on the

results.

In Sec. 2.2.2 we discuss the impurity ion deposition profiles, which can be properly taken into account by integrating Green's functions over the source coordinate.

Valuable information on the transport processes can be inferred by studying the temporal response of some spectroscopic signals in the case of short time puffing or pellet injection of impurities. For this purpose we discuss in Sec. 2.3 the time dependence of the solutions. By means of an eigenmode analysis the relations between various characteristic times are elucidated. Of great importance is the time constant τ_1 discussed in Sec. 2.3.2, which determines the decay or build-up of a stationary state. Finally, we treat for a simple case the propagation of an impurity pulse. The solutions are particularly of interest with respect to the plasma penetration probability for particles deposited in the scrape-off.

For the purpose of illustration we refer to ASDEX data. An application of the results to other devices should be possible without difficulties provided the relevant plasma parameters - in particular for the scrape-off region - are available. Some experimental findings on impurity transport in ASDEX are reported in Ref. /5/. More recent results including the impurity behaviour in the case of additional heating will be published in a forthcoming paper.

2. Impurity Transport Modelling

2.1 Model Equations

The starting point of our considerations is the continuity equation for an impurity species in ionization stage Z:

$$\frac{\partial n_Z}{\partial t} = -\mathrm{div}\ \vec{\Gamma}_Z + Q_Z - S_Z. \qquad (1)$$

In eq. (1) Q_Z and S_Z are the source and sink terms for the particles, which we do not need to specify in the following. As a next step we sum eq. (1) over all ionization states, thereby defining the total ion density

$$n^+ = \sum_{Z=1}^{N} n_Z,$$

and the total ion flux

$$\vec{\Gamma}^{+} \equiv \sum_{Z=1}^{N} \vec{\Gamma}_Z .$$

For the sum of the sources we have

$$\sum_{Z=1}^{N} Q_Z = \operatorname{div} \vec{\Gamma}_o ,$$

where $\vec{\Gamma}_o$ is the flux of neutrals.

Furthermore, we exclude the recombination to neutrals within the plasma. This approximation is in general well justified; exceptions may occur, however, in cases of extremely low temperatures ($T_e \lesssim 3$ eV) combined with high electron densities ($n_e \gtrsim 10^{13}$ cm^{-3}) and good confinement conditions ($D \lesssim 1000$ cm^2/s). Without such recombination processes the sum over all sinks of ions must vanish and we obtain instead of eq. (1)

$$\frac{\partial n^{+}}{\partial t} = -\operatorname{div} \vec{\Gamma}^{+} - \operatorname{div} \vec{\Gamma}_o . \qquad (2)$$

For the specification of the fluxes we adopt cylindrical coordinates, assuming a circular plasma cross-section; no toroidal or poloidal asymmetries will be considered. Within the region of closed magnetic surfaces $r \leq a$, we consider only perpendicular transport with the still quite general ansatz

$$\vec{\Gamma}^{+} = \sum_{Z=1}^{N} \left(-D_{\perp Z} \frac{\partial n_Z}{\partial r} + v_{\perp Z}\, n_Z\right) \vec{e}_r . \qquad (3)$$

This notation not only includes by means of the term $v_{\perp Z}\, n_Z$ the case of pressure-driven diffusion ($\Gamma_Z \propto \partial(n_Z T_Z)/\partial r$) but also allows one to consider the influence of other parameters (e.g. $\partial T_i/\partial r$, $\partial n_i/\partial r$ in neoclassical theory). On the other hand, anomalous diffusion is likely to be caused by fluctuating E-fields via E x B-drifts. In this case neither a Z nor an m_Z-dependence is to be expected. We therefore simplify expression (3) further by neglecting the Z-dependence of the transport quantities, which leads to

$$\vec{\Gamma}^{+} = \left(-D_{\perp} \frac{\partial n^{+}}{\partial r} + v_{\perp}\, n^{+}\right) \vec{e}_r . \qquad (4)$$

This expression has been found to describe the anomalous transport prevailing in the majority of experimental cases /5/ (a review is given in Ref./6/). It should be noted that relation (4) still offers a large measure of flexibility. For example, neoclassical transport may still be simulated owing to the dominant influence of the T_e-profile, which actually controls the radial charge

separation. In such a case the charge state abundance $f_Z = n_Z/\Sigma\, n_Z$ is first calculated over the plasma cross-section assuming corona equilibrium. The Z-dependence of the transport coefficients is then transferred into an r-dependence according to

$$D_\perp(r) = \Sigma\, f_Z(r)\, D_{\perp Z}(r),$$

$$V_\perp(r) = \Sigma\, f_Z\, V_{\perp Z}(r).$$

Using these coefficients we can finally calculate in a first order approximation of neoclassical transport the total ion density $n^+(r)$.

In the scrape-off region $a \leq r \leq r_w$ the additional fluxes parallel to the magnetic field become essential. For a discussion of the transport processes we refer to the following expression:

$$\vec{\Gamma}_Z = (-D_\perp \frac{\partial n_Z}{\partial r} + v_\perp\, n_Z)\, \vec{e}_r + (-D_{\parallel Z} \frac{\partial n_Z}{\partial s} + v_{\parallel Z}\, n_Z)\, \vec{e}_\parallel. \qquad (5)$$

There is little information from the experiments on the transport quantities in this region. With respect to the perpendicular part it is in particular uncertain whether the drift term $v_\perp n_Z$ exists at all in this zone of non-closed magnetic surfaces. The perpendicular diffusion, on the other hand, is experimentally substantiated for the background plasma from measured electron decay lengths

$$\lambda = -\left(\frac{d}{dr} \ln n_e\right)^{-1}\Big|_{r \geq a} \qquad (6)$$

and by studying deposition profiles of suprathermal protons on the neutralizer plates in ASDEX /7/. These experimental findings are compatible with the assumption of a constant diffusion coefficient of $D_\perp \approx D_\perp(r=a) = D_{\perp s}$. Moreover, because of the smallness of the scrape-off width $w = r - a$ (or, more specifically, λ, which in general is even smaller) in comparison with the minor radius, a weak radial dependence of $D_\perp$ is of little importance anyway. For the same reason the perpendicular drift term in eq. (5) may be neglected. This can be verified by comparing it with the perpendicular diffusion term, assuming $v_\perp(r \geq a) = V_{\perp a} = \text{const.}$:

$$\frac{V_\perp n_Z}{D_\perp dn_Z/dr} \sim \frac{|V_{\perp a}|d}{D_{\perp s}} = \frac{d}{a} \cdot \frac{|V_{\perp a}|a}{D_{\perp s}} \ll 1.$$

The ratio is much smaller than unity since the drift parameter

$$\alpha \equiv V_{\perp a} a/D_{\perp s} \qquad (7)$$

is typically of order one (see Sec. 2.2), whereas the ratio d/a with d = Min (λ,w) is in the range 0.1 - 0.01 for large devices like ASDEX (a = 40 cm, d $\lesssim$ 2 cm).

Addressing now the parallel fluxes in eq. (5), one has to realize that practically no direct information on the transport coefficients is available from the experiments. On the other hand, classical collision processes can be assumed to apply much better to the transport parallel to the field lines than for the strongly reduced transport perpendicular to them. Inserting the classical diffusion coefficient /8/

$$D_{\parallel Z} = \tau_Z \, kT_i/m_Z = \frac{3}{4} \, \frac{(kT_i)^{5/2}}{(2\pi m_i)^{1/2} \, e^4 Z^2 \ln\Lambda_i}$$

into eq. (5), we can compare the divergence of the parallel and perpendicular diffusion fluxes:

$$\frac{\frac{\partial}{\partial r} D_{\perp s} \frac{\partial n_Z}{\partial r}}{\frac{\partial}{\partial s} D_{\parallel Z} \frac{\partial n_Z}{\partial s}} \sim \frac{D_{\perp s}}{D_{\parallel Z}} \left(\frac{L_\parallel}{d}\right)^2 . \qquad (8)$$

In eq. (8) $L_\parallel$ is the characteristic length along the field lines. It is about half the distance between two absorbing surfaces (limiter or divertor plates) in the scrape-off and is of the order of the major torus circumference $2\pi R_o$ (ASDEX: R_o = 165 cm, $L_\parallel \approx$ 1500 cm). For typical scrape-off conditions (T_i = 15 eV, $n_i = 1 \times 10^{13}$ cm^{-3}, Z = 3, ln Λ_i = 20 and m_i = mass of proton) we get $D_{\parallel Z} = 7 \times 10^6$ cm^2/s, which must be compared with an anomalous value of $D_\perp \sim 6 \times 10^3$ cm^2/s. Because of $L_\parallel/d \sim 10^3$ we find that the right-hand side of eq. (8) is of order 10^3, which means that parallel diffusion can be neglected because of the very long gradient lengths. Any effec-

tive impurity exhaust parallel to the field line must therefore be attributed to the streaming term $v_{\parallel} n_Z$ in eq. (5). As discussed by Neuhauser /9/, the parallel streaming of the impurities is effected by three mechanisms: (1) friction forces, which tend to transport the impurity ions according to the streaming velocity of the background ions; (2) thermal forces ($\alpha \partial T_i/\partial s$), which tend to drive the particles back from limiters or neutralizer plates; and (3) electric forces ($\alpha \partial \Phi/\partial s$), which occur because of the electric potentials needed to establish ambipolarity of ion and electron fluxes.

Because of the various terms that influence the parallel transport, its evaluation would require information on the plasma parameters, such as temperatures, potentials and in particular the streaming velocity, as a function of the scrape-off coordinates, which are not available. For this reason and also for the sake of simplicity it has become common practice to replace the term div $\vec{\Gamma}_{\parallel}$ by a loss term $n^+ \tau_{\parallel}$, where $\tau_{\parallel}$ is the mean residence time for the impurity ions in the scrape-off region. One must be aware, however, that such a replacement is a rather rough simplification since in reality no particles are lost within the plasma volume. The description would be more appropriate to a situation - which is unlikely to be met in the experiments - where the particles rapidly bounce back and forth between the limiters or neutralizer plates with a small probability of absorption at the plates. All results based on this simplified treatment are therefore to be used with caution in the boundary region; they are at best correct in the sense that poloidal averaging has been applied. As far as the impurity ions are coupled to the flow of the background plasma by the friction forces, the residence time $\tau_{\parallel} = L_{\parallel}/v_{\parallel}$ can be estimated from the measured decay length λ of the electron density (eq. 6) by using the relations $\tau_{\parallel}^i = \tau_{\parallel}^e$, $D_{\perp s}^e = D_{\perp s}^i$ and

$$\lambda^2 = D_{\perp s} \cdot \tau_{\parallel}. \qquad (9)$$

Using equations (2), (4) and (5) and considering the smallness of the scrape-off width $w = r_w - a \ll a$, we finally end up with the following equations:

$$\text{I.} \quad \frac{\partial n^+}{\partial t} = \frac{1}{r} \frac{\partial}{\partial r} r\left[D_{\perp} \frac{\partial n^+}{\partial r} - v_{\perp} n^+\right] + Q_I(r), \qquad \text{for } r \leq a, \qquad (10a)$$

$$\text{II.}\quad \frac{\partial n^+}{\partial t} = D_{\perp s}\,\frac{\partial^2 n^+}{\partial r^2} - \frac{n^+}{\tau_{\shortparallel}} + Q_{II}(r), \qquad \text{for } a < r < r_w, \tag{10b}$$

Q_I and Q_{II} being the source terms -div $\vec{\Gamma}_o$ in the two regions.

2.2 Stationary Solutions

2.2.1 Green's Functions

We look for the stationary solutions of eq. (10) in the case where the flux of neutrals Γ_o (atoms/cm^2 s) originating from the wall is abruptly ionized within a shell of radius r' and r' + dr'. The corresponding source distribution is then presented by a delta function and we have to distinguish the two cases:

$$\text{case 1:}\quad r' \geq a, \qquad Q_I = 0, \qquad Q_{II} = \Gamma_o\,\delta(r-r'), \tag{11a}$$

$$\text{case 2:}\quad r' \leq a, \qquad Q_I = \Gamma_o \frac{a}{r'}\delta(r-r'), \qquad Q_{II} = 0\,. \tag{11b}$$

The solutions of eq. (10) are the Green's functions $n^+ = G_1(r,r')$ and $n^+ = G_2(r,r')$ in cases 1 and 2, repectively. They satisfy the homogeneous equations for $r \neq r'$:

$$\frac{d}{dr}\, r\,(D_\perp \frac{dG}{dr} - v_\perp\, G) = 0, \qquad 0 \leq r \leq a, \tag{12a}$$

$$\lambda^2\,\frac{\lambda^2 G}{dr^2} - G = 0\,, \qquad a \leq r \leq r_w\,, \tag{12b}$$

with $\lambda^2 = D_{\perp s}\,\tau_{\shortparallel}$. The fundamental solutions are

$$G = C_1\, e^F, \tag{13a}$$

$$G = C_2\, e^F \int \frac{e^{-F}}{\tilde{r} D_\perp}\, d\tilde{r}, \tag{13b}$$

with

$$F(r) = \int_0^r \frac{v_\perp(\tilde{r})}{D_\perp(\tilde{r})}\, d\tilde{r}, \tag{13c}$$

in the case of eq. (12a), and

$$G = C_3 \sinh(r/\lambda), \tag{13d}$$

$$G = C_4 \cosh(r/\lambda) \tag{13e}$$

for eq. (12b). By means of these functions the solution satisfying the following conditions has to be constructed:

$$\left.\frac{dG}{dr}\right|_{r=0} = 0, \tag{14a}$$

$$\lim_{\varepsilon \to 0}\{G(a-\varepsilon) - G(a+\varepsilon)\} = 0, \tag{14b}$$

$$\lim_{\varepsilon \to 0}\left\{D_{\perp a} \left.\frac{dG}{dr}\right|_{a-\varepsilon} - V_{\perp a}\, G(a-\varepsilon) - D_{\perp s} \left.\frac{dG}{dr}\right|_{a+\varepsilon}\right\} = 0, \tag{14c}$$

$$G(r_w) = 0, \tag{14d}$$

$$\lim_{\varepsilon \to 0}\{G(r'-\varepsilon) - G(r'+\varepsilon)\} = 0, \tag{14e}$$

and in addition

$$\lim_{\varepsilon \to 0}\left\{\left.\frac{dG_1}{dr}\right|_{r'-\varepsilon} - \left.\frac{dG_1}{dr}\right|_{r'+\varepsilon}\right\} = \frac{\Gamma_o}{D_{\perp s}}, \tag{14f}$$

or

$$\lim_{\varepsilon \to 0}\left\{\left.\frac{dG_2}{dr}\right|_{r'-\varepsilon} - \left.\frac{dG_2}{dr}\right|_{r'+\varepsilon}\right\} = \frac{a}{r'} \frac{\Gamma_o}{D_\perp(r')}. \tag{14g}$$

Condition (14a) is equivalent to $G(0) \neq \infty$; it also imposes a restriction on the drift velocity ($v_\perp < 0$ in the case of inward drift):

$$v_\perp(0) = 0 \quad \text{and} \quad \left.\frac{dv_\perp}{dr}\right|_{r=0} = 0. \tag{15}$$

With eq. (14d) we postulate complete absorption at the wall. Equations (14b) and (14c) provide the continuity of the density and ion fluxes at r = a. No discontinuity of the diffusion coefficient will be assumed, i.e. $D_{\perp a} = D_{\perp s}$ at r = a. At the source radius r = r' the density (G) is continu-

ous (14e) but the fluxes have to jump by Γ_o or Γ_o a/r' (eq. 14f, 14g).

In case 1, where the source is located in the scrape-off, the complete solution is given by:

$$G_1(r,r') = G_1(a,r') \begin{cases} e^{-\int_r^a \frac{v_\perp(\tilde{r})}{D_\perp(\tilde{r})}\,d\tilde{r}}, & 0 \le r \le a, \\ \cosh\left(\frac{r-a}{\lambda}\right), & a \le r \le r', \\ \dfrac{\cosh\left(\frac{r'-a}{\lambda}\right)}{\sinh\left(\frac{r_w-r'}{\lambda}\right)} \cdot \sinh\left(\frac{r_w-r}{\lambda}\right), & r' \le r \le r_w, \end{cases} \quad (16a)$$

with $\lambda = \sqrt{D_{\perp s}\tau_{\parallel}}$ and $w = r_w - a$ the scrape-off width. The density at the separatrix or limiter edge r = a is found to be

$$G_1(a,r') = \Gamma_o \frac{\lambda}{D_{\perp s}} \frac{\sinh\left(\frac{r_w-r'}{\lambda}\right)}{\cosh\left(w/\lambda\right)}. \quad (16b)$$

In the second case, with the sources located in the region of closed magnetic surfaces r' < a, we obtain the following result:

$$G_2(r,r') = G_2(a,r') \begin{cases} e^{F(r)}\left[e^{-F(a)} + \frac{aD_{\perp s}}{\lambda}\coth\left(\frac{w}{\lambda}\right)\int_{r'}^{a} \frac{e^{-F(\tilde{r})}}{D_\perp(\tilde{r})\tilde{r}}\,d\tilde{r}\right], & 0 \le r \le r', \\ e^{F(r)}\left[e^{-F(a)} + \frac{aD_{\perp s}}{\lambda}\coth\left(\frac{w}{\lambda}\right)\int_{r}^{a} \frac{e^{-F(\tilde{r})}}{D_\perp(\tilde{r})\tilde{r}}\,d\tilde{r}\right], & r' \le r \le a, \\ \dfrac{1}{\sinh\left(\frac{w}{\lambda}\right)} \cdot \sinh\left(\frac{r_w-r}{\lambda}\right), & a \le r \le r_w, \end{cases} \quad (17a)$$

with

$$G_2(a,r') = \Gamma_o \frac{\lambda}{D_{\perp s}} \tanh\left(\frac{w}{\lambda}\right) \quad (17b)$$

and F(r) according to eq. (13c). By combining eqs. (16) and (17) the density

on axis is found to be

$$G(0,r') = \frac{\Gamma_o \lambda}{D_{\perp s}} e^{-F(a)} \begin{cases} \sinh\left(\frac{r_w - r'}{\lambda}\right) / \cosh\left(\frac{w}{\lambda}\right), & r' \geq a, \\ \tanh\left(\frac{w}{\lambda}\right) + \frac{a D_{\perp s}}{\lambda} e^{F(a)} \int_{r'}^{a} \frac{e^{-F(\tilde{r})}\, d\tilde{r}}{D(\tilde{r})\, \tilde{r}}, & r' \leq a. \end{cases} \tag{18}$$

The ion fluxes to the wall $\Gamma_w^+ = -D_{\perp s}\, dG/dr\big|_{r=r_w}$ are

$$\Gamma_w^+ = \frac{\Gamma_o}{\cosh\left(w/\lambda\right)} \begin{cases} \cosh\left(\frac{r'-a}{\lambda}\right), & r' \geq a, \\ 1, & r' \leq a. \end{cases} \tag{19}$$

Our results may be visualized by considering a case of moderate inward drift velocity with a drift parameter of $\alpha = -2$ (eq. (7)) and $F(r) = -(r/a)^2$. The following set of data has been found appropriate for the description of the ohmic phase in D_2-discharges in ASDEX: a = 40 cm, w = 8 cm, $D_\perp = 4000\ cm^2/s$ = const., $\tau_\parallel = 1$ ms, $\lambda = \sqrt{D\tau_\parallel} = 2$ cm and $v_\perp = -200\ (r/a)$ cm/s.

In Fig. 1 we have depicted the two profiles $G_1(r, r' = 42\ cm)$ and $G_2(r, r' = 36\ cm)$. Characteristic of the first case is the peaking of the profile at the source location. This peaking is the more pronounced the smaller the penetration depth $s = r_w - r'$; it disappears for $s > w$. At $r = a$ the derivative jumps because of the discontinuity of $v_\perp$ ($v_\perp(r > a) = 0$). According to eq. (19) the fraction of Γ_w^+/Γ_o in the two cases is 0.057 and 0.037, respectively.

In Fig. 2 the central density according to eq. (18) is plotted as a function of the source radius with the inward drift velocity as a parameter (assuming $v_\perp/D_\perp = \alpha\ r/a^2$). The figure demonstrates the sensitivity of the impurity concentration to these variables. In Fig. 3a and 3b we show the same function for the parameters $\tau_\parallel$ and $D_\perp$ (assumed constant over the whole cross-section). Whereas in the former case a monotonic increase with $\tau_\parallel$ is found, the curves cross at a source location of $r' \sim 42$ cm for the latter parameter. The reason for this non-monotonic behaviour on $D_\perp$ can

be explained from the fact that with decreasing $D_\perp$ the particles are better confined - and driven to the centre by the inward drift - for large penetration depths ($r' \lesssim a$). For small penetration depths, however, the probability of reaching the region $r < a$ is reduced with decreasing $D_\perp$, thus resulting in an enhancement of the screening efficiency.

2.2.2 Ion Source Distributions

The basic equation for the determination of the radial distribution of the ion impurity sources is the continuity equation for the neutrals. With recombination into the neutral state again being neglected, this equation is given by

$$\frac{\partial n_o}{\partial t} = -\mathrm{div}\,\vec{\Gamma}_o - n_o\, n_e\, S_o, \tag{20}$$

where $S_o = S_o(T_e) = \langle \sigma_{io} v_e \rangle$ is the ionization rate coefficient for the neutrals. We consider the stationary case with cylindrical symmetry, putting $\Gamma_o(r) = -n_o v_o$ with $v_o > 0$ for the neutral flux density originating from the wall. The corresponding equation

$$\frac{1}{r\, n_o\, v_o}\, \frac{d}{dr}\,(r\, n_o\, v_o) = \frac{n_e\, S_o}{v_o} \tag{21}$$

can readily be integrated, yielding for the flux density versus radius

$$\Gamma_o(r) = -\, n_o\, v_o = -\,\Gamma_{ow}\, \frac{r_w}{r}\, e^{-\int_r^{r_w} \frac{n_e S_o}{v_o}\, d\tilde{r}}\,. \tag{22}$$

The source distribution of the ions is then found to be

$$Q(r) = -\mathrm{div}\,\vec{\Gamma}_o = |\Gamma_{ow}|\, \frac{r_w}{r}\, \frac{d}{dr}\, e^{-\int_r^{r_w} \frac{n_e S_o}{v_o}\, d\tilde{r}}\,. \tag{23}$$

In Sec. 2.2.1 the prefactor $|\Gamma_{ow}| \cdot r_w/r$ was already taken into account. (Note that because of the plane approximation used for the scrape-off the flux Γ_o is uncertain within the limits $|\Gamma_{ow}| \le \Gamma_o \le |\Gamma_{ow}| r_w/a$.)

We therefore have to use the normalized source function

$$q(r) = \frac{d}{dr} e^{-\int_r^{r_w} P(\tilde{r})d\tilde{r}} = P(r)\, e^{-\int_r^{r_w} P(\tilde{r})\, d\tilde{r}}, \qquad (24a)$$

with

$$P(r) = n_e(r) \cdot S_o(T_e(r))/v_o, \qquad (24b)$$

to calculate the total impurity density

$$n^+(r) = \int_o^{r_w} G(r,r')\, q(r')\, dr', \qquad (25a)$$

which for convenience may be subdivided into

$$n^+(r) = \int_o^a G_2(r,r')\, q(r')dr' + \int_a^{r_w} G_1(r,r')\, q(r')dr'. \qquad (25b)$$

The normalization of expression (24)

$$\int_o^{r_w} q(r)\, dr = 1 \qquad (25c)$$

is provided insofar as the plasma centre is inaccessible to the neutrals, i.e.

$$\exp(-\int_o^{r_w} P d\tilde{r}) \approx 0.$$

The above relations are only correct in cases where the flux of neutrals is both monodirectional and monoenergetic, a case which is generally not met in reality. To discuss the importance of the velocity and angular distributions, we consider the case of iron sputtering at the wall. According to Roth /10/ the distribution versus energy and angle of the sputtered Fe-atoms can be described by

$$f(E,\theta)\, dE \sin\theta\, d\theta = \text{const.} \left[\frac{E}{(E+E_o)^4}\right]^{2/3} \cdot \cos\theta\, dE \sin\theta\, d\theta,$$

with E_o = 1.5 eV. Introducing $\mu = \cos\theta$ and $w = E/E_o$ the normalized distribution function reads

$$f(w,\mu) = \frac{10}{3} \left[\frac{w}{(w+1)^4}\right]^{2/3} \mu, \qquad (26a)$$

with

$$\int_{w=0}^{\infty} \int_{\mu=0}^{1} f(w,\mu)\, dw\, d\mu = 1. \qquad (26b)$$

By means of eqs. (26a) and (24) the averaged source function is obtained from

$$\langle q(r)\rangle = P(r) \int_{o}^{\infty} \int_{o}^{1} e^{-\frac{1}{\mu\sqrt{w}} \int_{r}^{r_w} P\, d\tilde{r}} \cdot \frac{f(w,\mu)}{\mu\sqrt{w}}\, dw\, d\mu, \qquad (27)$$

with $P(r) = n_e S_o / v^*$ and $v^* = (2E_o/m_{Fe})^{1/2} = 2.3 \times 10^5$ cm/s. After integration over angles we are left with

$$\langle q(r)\rangle = P(r) \int_{o}^{\infty} E_2 \left[\frac{1}{\sqrt{w}} \int_{r}^{r_w} P\, d\tilde{r}\right] \cdot \frac{10}{3} \frac{w^{1/6}}{(w+1)^{8/3}}\, dw, \qquad (28a)$$

where $E_2(x) = \int_1^{\infty} e^{-xt} t^{-2} dt$ is the exponential integral of second order. By Substituting $w = t(1-t)$ eq. (28a) is brought into the more convenient form

$$\langle q(r)\rangle = \frac{10}{3} P(r) \int_{o}^{1} E_2 \left[\sqrt{(1-t)/t} \int_{r}^{r_w} P\, d\tilde{r}\right] t^{1/6} \sqrt{1-t}\, dt. \qquad (28b)$$

Our results are again illustrated by referring to ASDEX data of n_e and T_e boundary profiles. We distinguish the ohmic phase from the L and H-phases during neutral injection ($\bar{n}_e = 4 \times 10^{13}$ cm^{-3}, $I_p = 320$ kA, $B_T = 2.2$ T; L and H: $P_{NI} = 2.85$ MW; $H^o \rightarrow D^+$). The corresponding profiles shown in Fig. (4a) were taken from Ref. /11/; corrections of the order of $\Delta r \approx 1$ cm for the actual position of the separatrix were also taken into acocunt. In Fig. 4b we present the iron source functions before and after averaging according to eqs. (24) and (28b). The ionization rate coefficient S_o is calculated after Lotz /12/. In Fig. 4b we show in addition the source functions which are obtained after averaging over the angles only. It is found that averaging over the angles shifts the source profiles back towards the wall, whereas the averaging over velocity amplitudes has the opposite effect. After all, averaging results in a broadening of the source profiles. From Fig. 4 it is also obvious that in each of the three cases the ionic iron sources are located essentially in the scrape-off. In Fig.5 we plotted the integrand $G(0,r')\langle q(r')\rangle$ of eq. (25a) assuming in all three cases ohmic transport parameters as given in Sec. 2.2.1. The areas below the curves represent the iron density on axis.

For a flux density of $\Gamma_o = 1/\text{cm}^2\text{s}$ the densities at r = 0 are found to be $n^+_{OH} = 3.9 \times 10^{-4}$ cm^{-3}, $n^+_L = 2.6 \times 10^{-4}$ cm^{-3}, $n^+_H = 5.7 \times 10^{-4}$ cm^{-3}.

2.3 Time-dependent Solutions

2.3.1 General Properties of the Equations

Before treating more specific problems we elucidate some general features of time-dependent diffusion. To this end we revert to eq. (2) and specify the fluxes according to Sec. 2.1:

$$\frac{\partial n^+}{\partial t} = -\mathrm{div}\,(-\bar{\bar{D}}\,\mathrm{grad}\; n^+ + \vec{v}\, n^+) + Q(\vec{r}). \qquad (29)$$

Note that apart from switching on (or off) the sources Q at t = 0, no explicit time dependence is considered. For the following it is essential that the transport quantities $\bar{\bar{D}}$ (a tensor with components $D_\perp$ and $D_\parallel$) and $\vec{v}$ do not depend on n^+. This assumption will be justified for small impurity concentrations when the reaction on the background plasma can be neglected. In this case eq. (29) is a linear partial differential equation, which by means of the linear operator $L = \nabla \cdot (\bar{\bar{D}}\nabla - \vec{V})$ may be written as

$$\frac{\partial n^+}{\partial t} = L[n^+] + Q(\vec{r}). \qquad (30)$$

Since the right-hand side of this equation is independent of time and because of the lack of time derivatives higher than first order, one trivial consequence is the exclusion of oscillating solutions for $t \to \infty$.

2.3.1.1 Complementarity

In this section we prove the complementarity between impurity build-up and impurity decay.

Let us first consider impurity build-up. In this case we have the equation

$$\frac{\partial n_1^+}{\partial t} = L[n_1^+] + Q(\vec{r}), \qquad (31)$$

with the initial condition $n_1^+(0) = 0$ and the stationary solution $n_1^+(t \to \infty) = n_{st}(\vec{r})$.

Similarly, we have for the impurity decay

$$\frac{\partial n_2^+}{\partial t} = L[n_2^+]. \qquad (32)$$

The initial function, however, is now the stationary distribution $n_2^+(0) = n_{st}$. Adding eqs. (31) and (32), we obtain for $n = n_1^+ + n_2^+$ by virtue of the linearity of the operator L

$$\frac{\partial n}{\partial t} = L[n] + Q, \qquad (33)$$

with $n(0) = n_{st}$. Since n_{st} was defined as the stationary solution of eq. (31), which, however, is identical with eq. (33), we find $\frac{\partial n}{\partial t} \equiv 0$, or

$$n = n_1^+ + n_2^+ = \text{const.} \qquad (34)$$

The complementarity property expressed in relation (34) has been experimentally documented in ASDEX. In Fig. 6 we show the intensity of a ($\lambda = 499.4$ Å, Li-like) Si XII line (H_2 ohmic discharge, radiation peaking at plasma centre) when SiH_4 was puffed continuously during the time interval $0.715\ s \leq t \leq 1.115\ s$. Obviously, build-up and decay of Si in the discharge are governed by the same time constants. This property is of course expected in the case of pure diffusion transport; it is, however, not as obvious when additional streaming must be taken into account. Emphasizing the latter aspect we note that nothing can be learnt about inward or outward streaming by comparing the temporal behaviour of build-up and decay processes.

2.3.1.2 Eigenfunctions and Characteristic Times

In the last section we have seen that important information on the temporal behaviour of the solutions can be obtained from the decay of the profiles. Proceeding further along this line, we now look at the decay of the probability function G of a single particle. This again leads us to the concept of Green's function, which in the case of cylindrical symmetry has to satisfy (see eq. (10))

$$\frac{\partial G}{\partial t} = L[G], \qquad (35a)$$

with

$$L = \frac{1}{r}\frac{\partial}{\partial r}\, r\left(D_\perp \frac{\partial}{\partial r} - v_\perp\right) - \theta(r-a)/\tau_{\parallel}, \qquad (35b)$$

in which θ is the unit step function. In addition we have the initial condition

$$G(r,r',\ t = 0) = \delta(r-r')/2\pi r, \tag{35c}$$

which guarantees that for t = 0 there is one particle per unit length of the cylinder, and the boundary conditions

$$G(r_w,\ r',\ t) = 0, \qquad \left.\frac{\partial G}{\partial r}\right|_{r=0} = 0. \tag{35d}$$

Once $G(r,r',t)$ has been found, the solution for any source function $Q(r',t') = \Gamma_w(t') \cdot q(r')\ r_w/r'$ with q normalized according to (25c) can be obtained by integration (i.e. summing up the probabilities of the particles having been deposited at r = r' a time interval t-t' ago):

$$n^+(r,t) = \int_{-\infty}^{t} \int_{0}^{r_w} G(r,r',\ t-t') \cdot Q(r',t') \cdot 2\pi r'dr'dt'. \tag{36}$$

For Green's function we make the separation ansatz $G = e^{-\mu^2 D^* t/a^2} U(\rho)/a^2$ in eq. (35), where D^* is a characteristic value of $D_\perp$ and $\rho = r/a$. We are left with the radial equation

$$\frac{d}{d\rho}\ \rho\ \left(\frac{D_\perp}{D^*}\frac{dU}{d\rho} - \frac{V_\perp a}{D^*}\ U\right) + \left[\mu^2 - \theta(r-a)\ \frac{a^2}{\tau_{\shortparallel}\ D^*}\right]\ \rho U = 0. \tag{37}$$

In connection with the boundary conditions (35d) eq. (37) poses an eigenvalue problem of the Sturm-Liouville type /13/ (the transformation $U = y \cdot \exp\left(a \int v_\perp/D_\perp\ d\rho\right)$ yields a self-adjoint equation for y). The following properties are known:

a) The eigenvalues μ_n form an infinite set of discrete values: $\mu_1^2 < \mu_2^2 < \mu_3^2$ ... The eigenfunction U_n has (n-1) zeros in the interval $0 \leq \rho < 1$.

b) Orthogonality: In the above case one has for the normalized functions

$$\int_0^{\rho_w} U_n(\rho)\ U_m(\rho)\ \ 2\pi\rho\ d\rho = \delta_{nm}.$$

c) Completeness of the eigenfunctions:

$$\sum_{n=1}^{\infty} U_n(\rho) \cdot U_n(\rho') = \delta(\rho-\rho')/2\pi\ \rho'.$$

Owing to c) we immediately get

$$G(\rho,\rho',t) = a^{-2} \sum_{n=1}^{\infty} e^{-t/\tau_n} U_n(\rho')\, U_n(\rho), \tag{38a}$$

with the partial decay times

$$\tau_n = \frac{a^2}{\mu_n^2 D^*}. \tag{38b}$$

Because of property a) the time for build-up or decay of a stationary profile is essentially determined by τ_1.

By means of eq. (38) we are now in a position to discuss the relations between particle confinement times defined in different ways. We elucidate first the residence time of a particle. For this purpose we define the probability of a particle being found within the plasma after the time t has elapsed since its deposition at r = r':

$$P(r',t) \equiv \int_0^{r_w} G(r,r',t)\, 2\pi\, r\, dr. \tag{39}$$

Obviously, $|\dot{P}| = -dP/dt$ is the probability of losing the particle during the time interval t...t + dt. The residence time is consequently defined as the mean dwell time

$$\bar{t}(r') \equiv \int_0^{\infty} |\dot{P}|\, t\, dt. \tag{40a}$$

Because of $\lim_{t\to\infty} t\, P = 0$ we get by partial integration

$$\bar{t}(r') = \int_0^{\infty} P(r',t)\, dt. \tag{40b}$$

With eq. (38a) we obtain explicitly

$$\bar{t}(r') = \sum_{n=1}^{\infty} \tau_n\, U_n(r'/a) \int_0^{\rho_w} U_n(\rho)\, 2\pi\, \rho\, d\rho. \tag{41}$$

Another time constant frequently used to characterize the stationary condition is the particle replacement time, formally defined by

$$\tau_p = N/\Phi. \tag{42}$$

Here N is the number of particles within the plasma and $\Phi = \Gamma_w \cdot 2\pi\, r_w \cdot 2\pi\, R_o$ the total flux. For Φ = const. we obtain by means of eq. (36)

$$\tau_p = \int_0^{r_w} \int_0^{r_w} \int_{-\infty}^{t} G(r,r',t-t')\, q(r')dr'\, 2\pi\, r\, drdt', \qquad (43)$$

and by inserting eq. (38a)

$$\tau_p = \sum_{n=1}^{\infty} \tau_n \int_0^{r_w} U_n(r'/a)\, q(r')\, dr' \int_0^{\rho_w} U_n(\rho)\, 2\pi\, \rho\, d\rho. \qquad (44)$$

Putting $q = \delta(r-r')$ in eq. (44), we notice that the source specific replacement time $\tau_{rep}(r')$ is identical with $\bar{t}(r')$. We have thus shown that residence time and replacement time are identical in all cases. Both terms can therefore be united in the "particle confinement time":

$$\tau_p \equiv \tau_{rep} \equiv \bar{t}. \qquad (45)$$

In contrast to the decay time τ_1, which is essentially determined by the transport in the inner plasma region, τ_p largely depends on the source distribution q(r). There are obviously two ways for calculating τ_p: either from eq. (44) or, by returning to eq. (42), from the stationary solution. In the second way we obtain

$$\tau_p = \frac{1}{a\Gamma_o} \int_0^{r_w} \int_0^{r_w} G(r,r')\, q(r')\, dr'\, rdr, \qquad (46)$$

with G(r,r') according to eqs. (16),(17). We recognize in eq. (44) the Fourier series representation of eq. (46). An example of this relation is given in the next section.

The order of magnitude of τ_p can be estimated by considering the case $D_\perp$ = D = const. and $v_\perp$ = 0:

$$\tau_p(r') \sim \frac{1}{a\Gamma_o} \int_0^{a} G(r,r')\, rdr = \frac{a}{2\Gamma_o} G(0,r')$$

and by means of eq. (18)

$$\tau_p(r') \sim \frac{a\lambda}{2D} \begin{cases} \sinh\left(\frac{r_w - r'}{\lambda}\right) / \cosh\left(\frac{w}{\lambda}\right), & r' > a, \\ \tanh\left(\frac{w}{\lambda}\right) + \frac{a}{\lambda} \ln\left(\frac{a}{r'}\right), & r' < a. \end{cases} \qquad (47)$$

For $r' = a$ and $w \gg \lambda$ we obtain

$$\tau_p(r'=a) \sim \frac{a\lambda}{2D} = \frac{a}{2}\sqrt{\frac{\tau_{\shortparallel}}{D}} \,. \tag{48}$$

Thus, τ_p depends only linearly on the minor radius and weakly on D and $\tau_{\shortparallel}$. For ASDEX typical values of τ_p are in the range of 2 - 20 ms.

2.3.2 Hard-boundary Solutions in Cylindrical Geometry

Because of the complexity of eq. (37) time-dependent problems will in general require numerical treatment. However, in the case of inner-volume impurity sources (thermonuclear He production, impurity injection) as well as for the analysis of impurity decay a substantial simplification can be made by replacing the scrape-off region by an absorbing boundary ($\tau_{\shortparallel} \to 0$). In the following we derive some useful relations for the two basic cases $v_\perp = 0$ and $v_\perp \propto r$, assuming $D_\perp = D = \text{const}$.

2.3.2.1 Diffusion without Drift

For the cited conditions eq. (37) becomes Bessel's equation

$$\frac{d}{d\rho}\,\rho\,\frac{dU}{d\rho} + \mu^2 \rho\, U = 0. \tag{49}$$

Normalized solutions satisfying the boundary conditions $U(1) = 0$, $U(0) \neq \infty$ are

$$U_n(\rho) = \frac{J_o(\mu_n \rho)}{\sqrt{\pi}\, J_1(\mu_n)} \,, \tag{50}$$

with the zeros $\mu_1 = 2.4048$, $\mu_2 = 5.5200$ ... (see Refs. /14/, /15/ for numerical values and integral relations). The time dependent Green's function is thus given by

$$G(\rho, \rho', t) = \sum_{n=1}^{\infty} \frac{J_o(\mu_n \rho') \cdot J_o(\mu_n \rho)}{\pi\, J_1^2(\mu_n)}\, e^{-t/\tau_n} \,, \tag{51a}$$

with

$$\tau_n = \frac{a^2}{\mu_n^2 D} \tag{51b}$$

For $t > \tau_2 = 0.033\ a^2/D$ we have the approximation

$$G(\rho,\rho',t) \sim 1.18\, e^{-t/\tau_1} \left[J_o(\mu_1\rho') \cdot J_o(\mu_1\rho) + 2.33\, J_o(\mu_2\rho') \cdot J_o(\mu_2\rho)\, (e^{-t/\tau_1})^{5.29}\right]. \tag{51c}$$

The probability of finding the particle within the plasma after time t is

$$P(\rho',t) = \sum_{n=1}^{\infty} \frac{2}{\mu_n J_1(\mu_n)}\, J_o(\mu_n\rho')\, e^{-t/\tau_n}, \tag{52a}$$

with the approximation

$$P(\rho',t) \sim 1.60\, e^{-t/\tau_1} \left[J_o(\mu_1\rho') - 0.66 \cdot J_o(\mu_2\rho')\, (e^{-t/\tau_1})^{5.29}\right] \tag{52b}$$

For the confinement time we obtain according to eq. (41)

$$\tau_p(\rho') = \frac{2a^2}{D} \sum_{n=1}^{\infty} \frac{1}{\mu_n^3} \frac{J_o(\mu_n\rho')}{J_1(\mu_n)}\,. \tag{53}$$

For the same quantity a simple expression can be derived by returning to eq. (17) with $\lambda \to 0$

$$G(\rho,\rho') = -\frac{\Gamma_o\, a}{D} \begin{cases} \ln \rho', & \text{for } \rho \le \rho' \\ \ln \rho\ , & \text{for } 1 \ge \rho \ge \rho', \end{cases} \tag{54}$$

and applying eq. (46) with $q(r') = \delta(r-r')$:

$$\tau_p(\rho') = \frac{a^2}{4D}\,(1-\rho'^2)\ . \tag{55}$$

The identity of expressions (53) and (55) may be proved explicitly by developing $(1-\rho'^2)$ in a Fourier-Bessel series. From eq. (55) we learn in particular that the maximum confinement time for impurities deposited in the plasma centre is given by $\tau_p(0) = a^2/4D = 1.44\ \tau_l$.

2.3.2.2 Combined Diffusion and Drift

With $V_\perp = V_a \rho$ and $D_\perp = D = \text{const.}$ eq. (39) passes over into

$$\frac{d}{d\rho}\rho\left(\frac{dU}{d\rho} - \alpha\ \rho\ U\right) + \mu^2 \rho\ U = 0, \tag{56}$$

where the drift parameter $\alpha = V_a \cdot a/D$ has been introduced. The transformation $Z = \alpha\ \rho^2/2$ leads to

$$\frac{d}{dZ}\ \left[Z\ \left(\frac{dU}{dZ} - U\right)\right] + \frac{\mu^2}{2\alpha}\ U = 0, \tag{57a}$$

which alternatively may be cast into the self-adjoint form

$$\frac{d}{dZ}\ \left(Z\ e^{-Z}\ \frac{dU}{dZ}\right) - \left(1 - \frac{\mu^2}{2\alpha}\right)\ e^{-Z}\ U = 0 \tag{57b}$$

or the confluent hypergeometric form

$$Z\ \frac{d^2U}{dZ^2} + (1-Z)\ \frac{dU}{dZ} - \left(1 - \frac{\mu^2}{2\alpha}\right)\ U = 0. \tag{57c}$$

Solutions of (57c) are the confl. hypergeom. functions $M\left(1 - \frac{\mu^2}{2\alpha}, 1, Z\right)$. A more convenient form for $\alpha < 0$ is obtained by applying Kummer's relation /14/ $M(a,b,Z) = e^Z M(b-a, b, -Z)$, which leads to

$$U_n(\rho) = c_n\ e^{\frac{\alpha}{2}\rho^2}\ M\left(\frac{\mu_n^2}{2\alpha}, 1, -\frac{\alpha}{2}\ \rho^2\right). \tag{58a}$$

The series representation of M reads in this case

$$M = 1 + \sum_{\nu=1}^{\infty} (-1)^\nu\ \frac{\left(1+\frac{2\alpha}{\mu_n^2}\right)\left(1+2\ \frac{2\alpha}{\mu_n^2}\right)\ldots\left(1+(\nu-1)\ \frac{2\alpha}{\mu_n^2}\right)}{(\nu!)^2}\ \left(\frac{\mu_n \rho}{2}\right)^{2\nu}. \tag{58b}$$

The two smallest eigenvalues μ_1^2, μ_2^2 calculated from $M(\rho = 1) = 0$ are plotted in Fig. 7 as a function of α. We see that μ_2^2 is nearly constant, thus leading to $\tau_2 \sim 0.03\ a^2/D$, whereas μ_1^2 increases approximately exponentially as a function of α. The decay (or build-up) time constant

$$\tau_1 = \frac{a^2}{\mu_1^2 D} \sim 0.173\ e^{-0.17\alpha}\ a^2/D \qquad (59)$$

is thus increased in the case of an inward drift ($\alpha < 0$) and decreased for outward drifting particles.

In the two cases $\alpha = \pm 2$ the first eigenfunctions are elementary. Below we give these normalized functions and also the probability (defined by eq. (39)) of finding the particle in the plasma after time $t \gtrsim \tau_2$.

Inward drift $\alpha = -2$: $\tau_1 = a^2/4D$; $\tau_2 = 0.14\ \tau_1$

$$U_1(\rho) = \frac{2}{\sqrt{\pi(1-e^{-2})}}\ (1-\rho^2)\ e^{-\rho^2}, \qquad (60)$$

$$P(\rho',t) \sim 1.70\ (1-\rho'^2)\ e^{-\rho'^2} \cdot e^{-t/\tau_1}. \qquad (61)$$

Outward drift $\alpha = +2$: $\tau_1 = a^2/8D$; $\tau_2 = 0.24\ \tau_1$

$$U_1(\rho) = \sqrt{\frac{3}{\pi}}\ (1-\rho^2), \qquad (62)$$

$$P(\rho',t) \sim 1.50\ (1-\rho'^2)\ e^{-t/\tau_1}. \qquad (63)$$

For illustration we apply the above results to an impurity injection experiment. Figure 8 shows the decay in intensity of the H-like Ne X line ($\lambda = 12.13$ Å) emitted from the plasma centre. The neon was injected into an ASDEX D_2 ohmic discharge by means of a doped D_2 pellet (~1 % Ne) which reached approximately half the minor radius. We see that already 20 ms

after injection the intensity shows a slow exponential decay with a time constant τ_1 = 75 ms. The time needed for establishing the ionization equilibrium is estimated at $\tau_{ion} = (S_X\, n_e)^{-1} \lesssim 10$ ms. After this time the measured intensity of the NeX line is representative for the total ion density. After 250 ms the signal has attained the stationary level caused by the recycling of the particles from the divertor (pumping can be neglected on this time scale). From the measurement of τ_1 the diffusion coefficient can be determined provided additional information on the drift is available. This can be obtained in principle from measurements of the impurity density profiles, which, however, cannot be performed with the desired accuracy because of VUV calibration and other spectroscopic problems. For this reason there is an uncertainty with respect to the drift, which for the ohmic phase is estimated to be in the range $-2 \leq \alpha \leq 0$. By means of relation (59) we thus get D within the limits 3700 - 5900 cm^2/s. The time constant τ_2 is found to be in the range 14 - 24 ms, which is in agreement with the observation that for $t \gtrsim 20$ ms only the first eigenmode is of importance. This is shown more specifically by means of eq. (52b) on the assumption of an effective deposition radius of $\rho' = 0.6$:

$$\alpha = 0\text{: } P(t) \sim 0.87 \cdot e^{-t/\tau_1} + 0.37 \cdot e^{-t/\tau_2}$$

In case of an inward drift we get from eq. (61)

$$\alpha = -2\text{: } P(t) \sim 0.76 \cdot e^{-t/\tau_1}$$

The fraction of neon atoms remaining in the plasma at the end of the decay phase after t = 200 ms is thus estimated at 5 % - 6 %. We notice that the influence of drift on this result is rather small. The consideration of the proper deposition profile, however, can have a much greater impact on the result.

2.3.3 Impurity Penetration Probability and Screening

During the stationary phase there is zero net flux of particles within the regions without sources. This vanishing flux is actually provided by balanced ingoing and outgoing fluxes. The magnitude of these balanced fluxes cannot be obtained from the stationary solutions but require a time-dependent treatment of the transport problem. The quantity of interest in this context is the penetration probability $P(r)$. By means of this quantity the outward fluxes are found to be $\Phi^{+}_{out}(r) = \Phi_o P(r)$, with Φ_o being the incoming flux of neutrals. $P(r)$ is defined as the temporal maximum of the containment probability of a neutral flux particle within the region of radius r. More specifically, we define for a given source radius r' as in eq. (39)

$$P(r,r') = \begin{cases} P(r,r',t_{max}), & \text{for } r' > r \\ 1 & \text{for } r' \leq r \end{cases} \qquad (64a)$$

with

$$P(r,r',t) = \int_o^r G(\tilde{r},r',t)\, 2\pi\, \tilde{r}\, d\tilde{r} \qquad (64b)$$

assuming $r' > r$, and

$$\frac{\partial}{\partial t} P(r,r',t)\Big|_{t_{max}} = 0. \qquad (64c)$$

$P(r)$ is finally obtained by a further integration over the source distribution (eq. (27a)):

$$P(r) = \int_o^{r_w} P(r,r')\, q(r')\, 2\pi\, r'\, dr'. \qquad (65)$$

In particular, $P(a)$ is the probability of penetration into the region of closed magnetic surfaces. Conversely, the fraction $P_s = 1 - P(a)$ of the neutral flux is lost directly from the scrape-off region; P_s is consequently termed as the screening efficiency of the scrape-off.

We now prove the cited relation between the penetration probability and stationary outward flux. It should first be noted that the outward flux at radius $r < r'$ is to be attributed to particles that have entered the discharge at times $t < t_{max}(r)$. On the other hand, particles which entered at $t > t_{max}$ contribute to

the balanced inward flux. We thus have

$$\Gamma^{+}_{in}(r) = (-D \frac{\partial}{\partial r} + v_{\perp}) \int_{0}^{t_{max}} 2\pi\, r'\, \Gamma_o \cdot G(r,r',t)\, dt \qquad (66a)$$

and

$$\Gamma^{+}_{out}(r) = (-D \frac{\partial}{\partial r} + v_{\perp}) \int_{t_{max}}^{\infty} 2\pi\, r' \Gamma_o \cdot G(r,r',t)\, dt. \qquad (66b)$$

Applying the operator $1/r\ \partial/\partial r\ r$ on both sides and assuming $r \leq a$, we get by means of the differential equation (35)

$$\frac{1}{r} \frac{\partial}{\partial r}\ r\ \Gamma^{+}_{out} = -2\pi\, r'\, \Gamma_o \int_{t_{max}}^{\infty} L[G]dt = -2\pi\, r'\, \Gamma_o \int_{t_{max}}^{\infty} \frac{\partial G}{\partial t}\, dt,$$

$$\frac{\partial}{\partial r}\, r\, \Gamma^{+}_{out} = 2\pi\, r'\, \Gamma_o\, G(r,r',t_{max}) \cdot r.$$

A further integration over r leads to our desired result (taking into account $t_{max} = 0$ for $r' < r$ and $G(\tilde{r},r',0) = \delta(\tilde{r},r')/2\pi\, r'$):

$$\Phi^{+}_{out} = \Phi_o \{ \int_{0}^{r< r'} G(\tilde{r},r',t_{max})\, 2\pi\, \tilde{r}\, d\tilde{r} + \theta(r-r') \}\ . \qquad (67)$$

We elucidate the above quantities by referring to a simplified soft-boundary problem. We assume: linear geometry with no absorbing walls, $D_{\perp}$ = const, $v_{\perp} \equiv 0$. Closed magnetic surfaces are within the region $-a \leq x \leq +a$; the scrape-off layer with a mean residence time $\tau_{\parallel}$ extends from $|x| > a$ to infinity. Equation (35) is thus simplified to

$$\frac{\partial G}{\partial t} = D \frac{\partial^2 G}{\partial x^2} - \theta(|x| - a)\, G/\tau_{\parallel}. \qquad (68)$$

We are looking for even solutions $G(x) = G(-x)$ with $\int_{o}^{\infty} G^2\, dx \neq \infty$, and with G and $\partial G/\partial x$ continuous at $x = a$. The separation ansatz $G = e^{-\mu^2 Dt/a^2} U(\xi)$ with $\xi = x/a$ leads to

$$0 = \frac{d^2U}{d\xi^2} + \mu^2 U, \qquad \text{for} \quad |\xi| \leq 1,$$

$$0 = \frac{d^2U}{d\xi^2} + (\mu^2 - K_o^2)U, \qquad \text{for} \quad |\xi| > 1, \tag{69}$$

with $K_o^2 = a^2/D\,\tau_{\shortparallel}$ (i.e. $K_o = a/\lambda$, with λ being the decay length).

For $\mu^2 \leq K_o^2$ we get a finite set of discrete solutions:

$$U_n(\xi) = A_n \begin{cases} \cos(\mu_n \xi), & |\xi| \leq 1, \\ \cos \mu_n \cdot e^{-\sqrt{K_o^2 - \mu_n^2}\,(|\xi| - 1)}, & |\xi| > 1. \end{cases} \tag{70a}$$

Continuity of the derivative at $\xi = 1$ yields the equation for the eigenvalues $\mu_n \sin \mu_n = \cos \mu_n \cdot \sqrt{K_o^2 - \mu_n^2}$, which is equivalent to

$$|\cos \mu_n| = \mu_n / K_o \tag{70b}$$

with the secondary condition $\tan \mu_n > 0$. The solutions of eq. (70b) are illustrated in Fig. (9) for the case $K_o = 20$. We realize that the number of discrete eigenvalues is given by $N = 1 + \mathrm{INT}(K_o/\pi)$. With $K_o \to \infty$ ($\tau_{\shortparallel} = 0$), we obtain the hard-boundary case with $\mu_n = (2n-1)\,\pi/2$, $n = 1, 2 \ldots \infty$. The pre-factor A_n is determined by normalization to

$$A_n = (1 + 1/\sqrt{K_o^2 - \mu_n^2})^{-1/2}\,. \tag{70c}$$

The orthonormality relation $\int_{-\infty}^{\infty} U_n\, U_m\, d\xi = \delta_{nm}$ for the above functions may be proved explicitly.

For $\mu^2 > K_o^2$ the solutions of eq. (69) are given by

$$U(k,\xi) = B_k \begin{cases} \cos(\mu\,\xi), & |\xi| \leq 1 \\ \cos \mu \cdot \cos[k(|\xi| - 1)] - \frac{\mu}{k} \sin k \cdot \sin[K(|\xi| - 1)], & |\xi| > 1, \end{cases} \tag{71a}$$

with $k = \sqrt{\mu^2 - K_o^2}$. There are no further conditions in this case for selecting the eigenvalues. Hence, the values of k provide a continuous spectrum with $0 \leq k \leq \infty$. The pre-factor B_k now has to be determined as a functon of k from the orthonormality condition

$$\int_{-\infty}^{\infty} d\xi\, U(k,\xi) \cdot U(k',\xi) = \delta(k-k'), \tag{71b}$$

leading to

$$\lim_{\Delta k \to 0} \int_{-\infty}^{\infty} d\xi \; U(k,\xi) \int_{k-\Delta k}^{k+\Delta k} dk' \; U(k',\xi) = 1. \tag{71c}$$

This latter relation yields

$$B_k = [\pi \, (1 + \frac{K_o^2}{k^2} \sin^2\mu)]^{-1/2}. \tag{71c}$$

Finally, we obtain Green's function analogously to eq. (38a):

$$G(\xi, \xi', t) = \sum_{n=1}^{N} e^{-\mu_n^2 t/\tau_o} U_n(\xi) \, U_n(\xi') + \tag{72}$$

$$+ e^{-K_o^2 t/\tau_o} \int_o^{\infty} e^{-k^2 t/\tau_o} U(k,\xi) \, U(k,\xi') \, dk \, ,$$

with $G(\xi,\xi',0) = 1/2\ \delta(\xi-\xi') + 1/2\ \delta(\xi+\xi')$ and $\tau_o = a^2/D$. Because of $K_o^2\ t/\tau_o = t/\tau_{\prime\prime}$ the continuous part is of importance only for short times $t \lesssim \tau_{\prime\prime}$. Nevertheless, this portion is essential for calculating the screening probability since it describes the initial broadening and decay of the probability function in the scrape-off.

We demonstrate the solution given by eq. (72) by the reference set of data: $a = 40$ cm, $D = 4000\ \mathrm{cm}^2/\mathrm{s}$, $\tau_{\prime\prime} = 1 \times 10^{-3}$ s (i.e. $K_o = 20$, $\lambda = 2$ cm, $\tau_o = 0.4$ s, $\tau_1 = \tau_o/\mu_1^2 = 0.18$ s). The source coordinate chosen is $|\xi'| = 1.1$, i.e. two decay lengths away from the region of closed surfaces.

Figure (10) shows the function G together with its discrete and continuous parts as a function of ξ for $t = \tau_{\prime\prime}$ (the integral in eq. (72) is easily evaluated by means of standard numerical methods). We see that the discrete and continuous fractions cancel exactly in the inner region. Figure (11) depicts the development of the probability function G in steps of time $t_m = \tau_{\prime\prime}\ 2^{m-1}$; for the purpose of presentation the corresponding curves have been multiplied by 2^{m-1} ($m = 1,2,3 \ldots$).

We recognize from Fig. (11) an inward diffusion into the region $|\xi| \leq 1$ for a period $t \lesssim 2\,\tau_{\perp\perp} \approx t_{max}$. Thereafter, this flux changes into an outward flux because of the propagation of the pulse into the interior region. The penetration probability is given by the area left of the pulse maximum. After $t \sim 128$ ms $= 0.7\,\tau_1$ only the fundamental mode $n = 1$ of eq. (72) is left and the profiles decay without a further change of shape.

To calculate the penetration probability, expression (72) is integrated:

$$P(\xi,\xi',t) = 2 \int_0^{\xi} G(\tilde{\xi},\xi',t)\, d\tilde{\xi}. \tag{73}$$

This integration consists in replacing the functions $U_n(\xi)$ and $U(k,\xi)$ in eq. (72) by

$$W_n(\xi) = \frac{2A_n}{\mu_n} \begin{cases} \sin(\mu_n\,|\xi|), & |\xi| \leq 1 \\ \sin\mu_n + \dfrac{\mu_n \cos\mu_n}{\sqrt{K_o^2-\mu_n^2}} \left(1 - e^{-\sqrt{K_o^2-\mu_n^2}\,(|\xi|-1)}\right), & |\xi| > 1 \end{cases} \tag{74a}$$

and

$$W(k,\xi) = \frac{2B_k}{\mu} \begin{cases} \sin(\mu\,|\xi|), & |\xi| \leq 1 \\ \sin\mu + \dfrac{\mu^2}{K^2}\,\sin\mu\,[\cos(K|\xi|-1)-1] + & \\ + \dfrac{\mu}{K}\cos\mu \cdot \sin(K|\xi|-1), & |\xi| > 1. \end{cases} \tag{74b}$$

The maximum of the function $P(\xi,\xi',t)$ is obtained at time $t = t_{max}$, with t_{max}/τ_o being a function of the variables ξ, ξ' and K_o. For this reason the penetration probability $P(\xi, \xi', t_{max})$ is - in the simplified case considered - only a function of the same three variables. In Fig. 12 we have plotted $P(\xi, \xi', K_o)$ as a function of K_o with ξ and ξ' as parameters. We see from the figure that the penetration probability is a monotonically decreasing function of $K_o = a/\sqrt{D\,\tau_{\perp\perp}}$. For the penetration into the inner region $|\xi| \leq 1$ we obtain for a typical case ($K_o = 20$, $\xi' = 1 + \sqrt{D\tau_{\perp\perp}} = 1.05$)

a probability of 14 %. Under the same conditions the peneration probability into the core region $|\xi| \leq 0.5$ amounts to 1.6 %. In this latter case the penetration probability for $|\xi'| \neq 1$ can be estimated from the curve shown in Fig. 12 by noting that $t_{max}/\tau_o \approx$ const. and considering only the lowest mode n = 1. This leads to

$$P(0.5, \xi', K_o) = P(0.5, \xi', K_o) \cdot U_1(\xi')/U_1(1),$$

which for $|\xi'| > 1$ results in a reduction factor of $\exp [-K_o(|\xi'|-1)]$.

We finally notice that an increase of the penetration probability does not necessarily lead to increased impurity densities. In fact, we have found in Sec. 2.2 (Fig. 3b) that the stationary concentration is reduced with growing D for source locations close to the separatrix. On the other hand, the penetration probability is seen in Fig. 12 to increase monotonically with D. This paradoxical behaviour can be understood by referring to Fig. 13, which shows the residence probability $P(\xi = 0.8, \xi' = 1., t)$ as a function of time with the two values D = 4,000 and 10,000 cm^2/s as parameters. We see that the penetration probability - the maxima of the curves - is higher for the larger value of D. However, the particle confinement time, which is represented by the area under the curve (eq. (40b)), is smaller in this case. These relations may be described as follows: In the case of low-diffusivity the screening efficiency is high and most of the particles are lost directly from the scrape-off. The small fraction of particles, however, that reaches the inner plasma region is confined for long times. Conversely, in the case of high D, the particles first penetrate into the plasma but leave it after a short time. For this reason the ionization state of the outgoing particle flux in the scrape-off will rise with increasing D.

3. Summary

When discussing impurity problems, it is appropriate to distinguish between four processes: production, penetration of the neutrals, transport in the scrape-off layer, and transport in the inner region of closed magnetic surfaces. In the preceding sections we have studied the importance of the last three processes. Because of the assumption of cylindrical symmetry our treatment is suitable for impurities homogeneously produced at the walls (e.g. by charge exchange sputtering). For limiter-produced impurities it is probably necessary to have a more refined description - particularly in the case of small penetration ranges of the neutrals - that takes into account the possibility of particle re-deposition on the limiter.

The basic equations (10a) and (10b) were derived on the assumption of anomalous transport over the whole plasma cross-section. The transport of the particles perpendicular to the magnetic surfaces is described by combined diffusion and streaming, with $D_\perp$ and $v_\perp$ being arbitrary functions of the radius. This ansatz provides the necessary flexibility for simulating experimental observations; it is also appropriate for approximate description of neo-classical transport. The weakest point in our analysis is presumably the parallel transport in the scrape-off, for which no direct information from the experiments exists. The parallel losses are characterized by a scrape-off residence time $\tau_\parallel$. In addition to $D_{\perp s}$, the diffusion coefficient in the scrape-off, and the functions $D_\perp(r)$ and $v_\perp(r)$, this time is another parameter which may change when the experimental conditions are varied.

For stationary conditions the impurity density at the plasma center is given by Green's function according to eq. (18), it being assumed that the given flux of neutral impurity atoms is ionized at a fixed radius r'. This expression may be used for a rough estimation of the impurity density. Furthermore, it is suitable for discussing the influence of the transport quantities and the scrape-off width w. The inner transport parameters yield a factor $\exp\left(-\int_0^a v_\perp/D_\perp \, dr\right)$. In the case of inward drifting particles ($v_\perp < 0$), this factor describes the impurity accumulation in the plasma center. For small drift velocities the impurity density on axis becomes independent of both the inner transport parameters $v_\perp$ and $D_\perp$. In this case it is completely determined by the boundary quantities $D_{\perp s}$, $\tau_\parallel$ and w and the penetration depth $s = r_{wall} - r'$. These parameters contribute the important

factor sinh $(s/\sqrt{D_\perp \tau_\parallel})$ in eq. (18). An increase of the penetration depth - scaled to the decay length $\lambda = \sqrt{D_\perp \tau_\parallel}$ (typically 1-2 cm) - thus results in a nearly exponential rise of the impurity concentration. This sensitivity to the penetration depth emphasizes the importance of the edge T_e and n_e profiles. These profiles determine via eq. (24b) the ionic source distribution q(r). Equation (24a) gives this deposition profile for monoenergetic, radially inward flying particles. For the case of sputtered Fe-atoms we also investigated the influence of the velocity distribution. The tail of the velocity distribution is of particular importance because of the large penetration depth of the high-velocity particles. After all, it is found that the monoenergetic, monodirectional approximation is already quite suitable since the effect of long-ranging tail particles is compensated to a great extent by an increase of the opacity when the isotropy of the distribution is taken into account. Inserting the source term (28) into eq. (25) gives the final result of the stationary problem. For small penetration depth $s \ll a$, the concentration on axis is practically independent of the minor radius a.

In the discussion of time-dependent problems, we concentrated mainly on the general features of the solutions. A function comprising all of the general features is the time-dependent Green's function, which describes the propagation and decay of a δ-pulse of particles. By means of expression (38) we could show that the different formulations of the particle confinement time τ_p (i.e. residence time and replacement time) are actually identical. This characteristic time can already be obtained from the stationary solution by applying definition (42). For the impurities this confinement time is again largely determined by the edge parameters; it is found to increase only linearly with the minor radius.

Another important time constant is the decay time τ_1 this being in general much larger than τ_p. This time constant is characteristic of the build-up or decay of a stationary impurity level. According to eq. (38b) it is independent of the source location and rises proportionally to a^2/D^*, with D^* being a characteristic value of the diffusion coefficient in the inner plasma region. Equation (59) gives τ_1 for the case of combined diffusion and radial drift. It is found that the build-up (or decay) of a stationary impurity density is prolonged in the case of an inward drift. This prolongation is evidently caused by the concomitant rise of the stationary level.

In the last section we elucidated the problems of diffusive penetration and screening, which also require a time-dependent treatment. For the simplest case of linear geometry an explicit expression for Green's function is derived (eq. 72). The solution consists of a finite number of discrete eigenstates and a continuum part. The transition from free-boundary to hard-boundary relations is seen to take place at times $t \gtrsim \tau_{\parallel}$, when the continuum part becomes negligible. By means of solution (72) typical screening efficiencies of >80 % were calculated for particle deposition at $r' = a + \lambda$.

The probability of reaching the core plasma ($r/a \leq 0.5$) is typically in the range of 1 %. The screening efficiency is reduced with increasing D. Such a reduction of screening, however, does not inevitably lead to enhanced impurity densities. For source locations in the inner region and close to the separatrix the opposite effect was found, which can be explained by a reduction of the particle confinement time.

In comparison with numerical code calculations - based on the same formulation of transport - our analytical results suffer from the fact that they do not present the distribution of the various charge states over the plasma cross-section, but rather give the sum over all ionic states. For the evaluation of experimental data numerical calculations are therefore indispensable. On the other hand, the advantage of an analytic analysis is that it provides us with a deeper understanding of the problem. A closed analytic expression ultimately allows optimum orientation in a multi-dimensional parameter space. Such orientation is in turn an indispensable prerequisite for reasonable numerical work.

Acknowledgements

The cooperation of the ASDEX team in the experiments is gratefully acknowledged. These investigations have been stimulated by discussions with Drs. K. Behringer and W. Engelhardt. In particular the numerical transport code developed by K. Behringer had a great impact on this work.

References

/1/ W. Engelhardt and W. Feneberg, J. Nucl. Mater. 76 & 77, 518 (1978)

/2/ W. Engelhardt et al., J. Nucl. Mater. 111 & 112, 337 (1982)

/3/ K. Lackner and D. Post, in Physics of Plasma-Wall Interactions in Controlled Fusion (Behrisch, R., Post, D., Eds.) Nato Advanced Study Institutes Programme, Val. Morin, Canada (1984).

/4/ M. Keilhacker et al., Proc. 10th Inter. Conf. on Plasma Physics and Contr. Nucl. Fus. Research, London (1984), IAEA-CN-44/A II-1

/5a/ K. Behringer, W. Engelhardt, G. Fussmann and the ASDEX team, paper I.C.6, Proceedings of the IAEA Technical Committee Meeting on Divertors and Impurity Control, Garching (1981).

/5b/ K. Behringer, G. Fussmann, W. Poschenrieder et al., 11th Europ. Conference on Controlled Plasma Physics, paper C27, Aachen (1983) (the third page is missing in the proceedings; the complete paper is available on request).

/6/ R.C. Isler, Nucl. Fus., 24, 12, 1599-1668 (1984)

/7/ F. Wagner, Nucl. Fus., 25, 5, 525 - 536 (1985)

/8/ L. Spitzer, Physics of Fully Ionized Gases, 2nd Edition; Interscience Publishers, N.Y. (1962)

/9/ J. Neuhauser et al., Nucl. Fus. 24, 1, 39 - 47 (1984)

/10/ J. Roth, see Ref. /3/

/11/ K. Lackner et al., see Ref. /4/, paper IAEA-CN-44/A-V-4

/12/ W. Lotz, Astrophys. J. Suppl. 128, 207 (1967)

/13/ W. Gröbner, P. Lesky, "Mathematische Methoden der Physik II" Bibliographisches Institut, Mannheim (1965)

/14/ M. Abramowitz, I.A. Stegun, "Handbook of Mathematical Functions", Dover Publications, N.Y. (1970)

/15/ I.N. Sneddon, "Spezielle Funktionen der Mathematischen Physik", Bibliographisches Institut, Mannheim (1963)

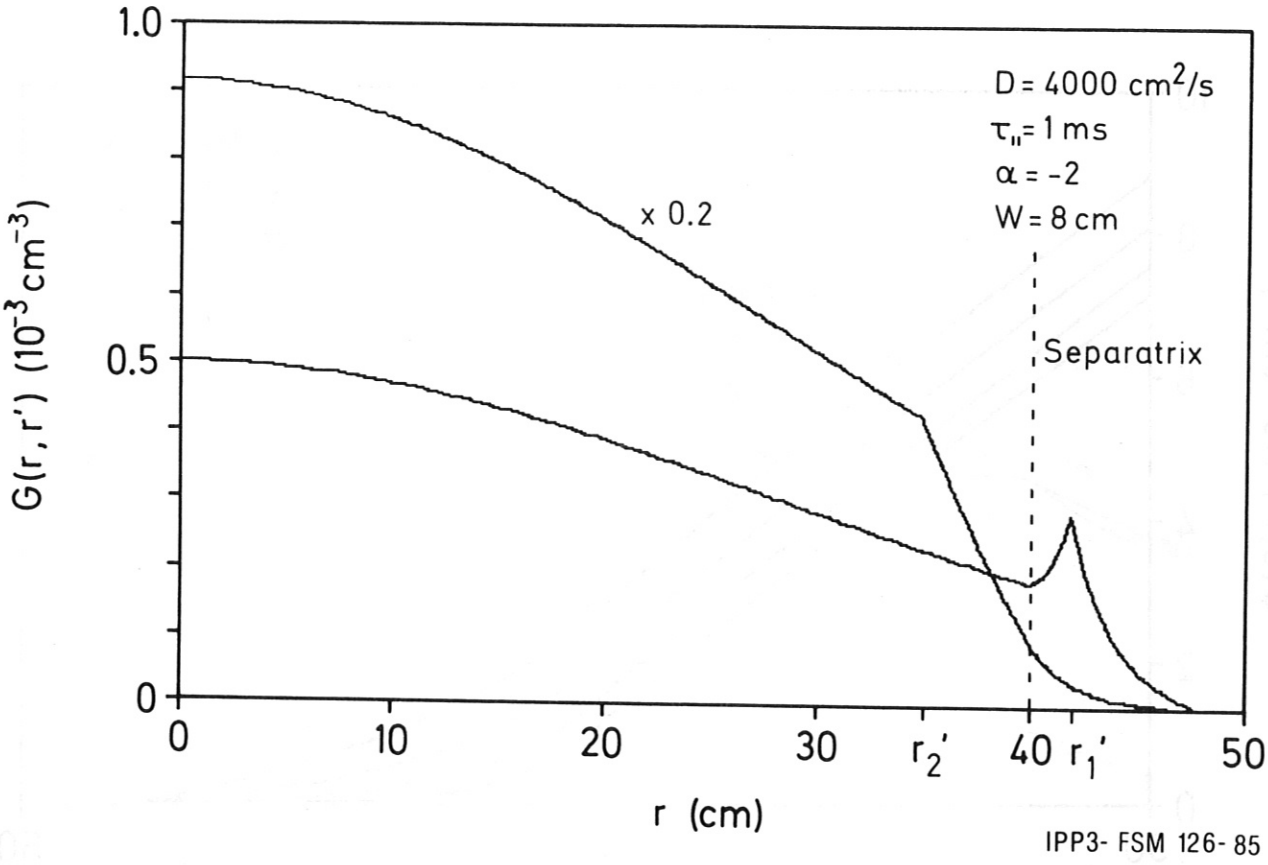

Fig. 1: Impurity density G(r,r') as a function of radius r for the source positions r'_1 = 42 cm and r'_2 = 35 cm ($v_\perp$ = 200 r/a cm/s, Γ_o = 1 cm^{-2} s^{-1}).

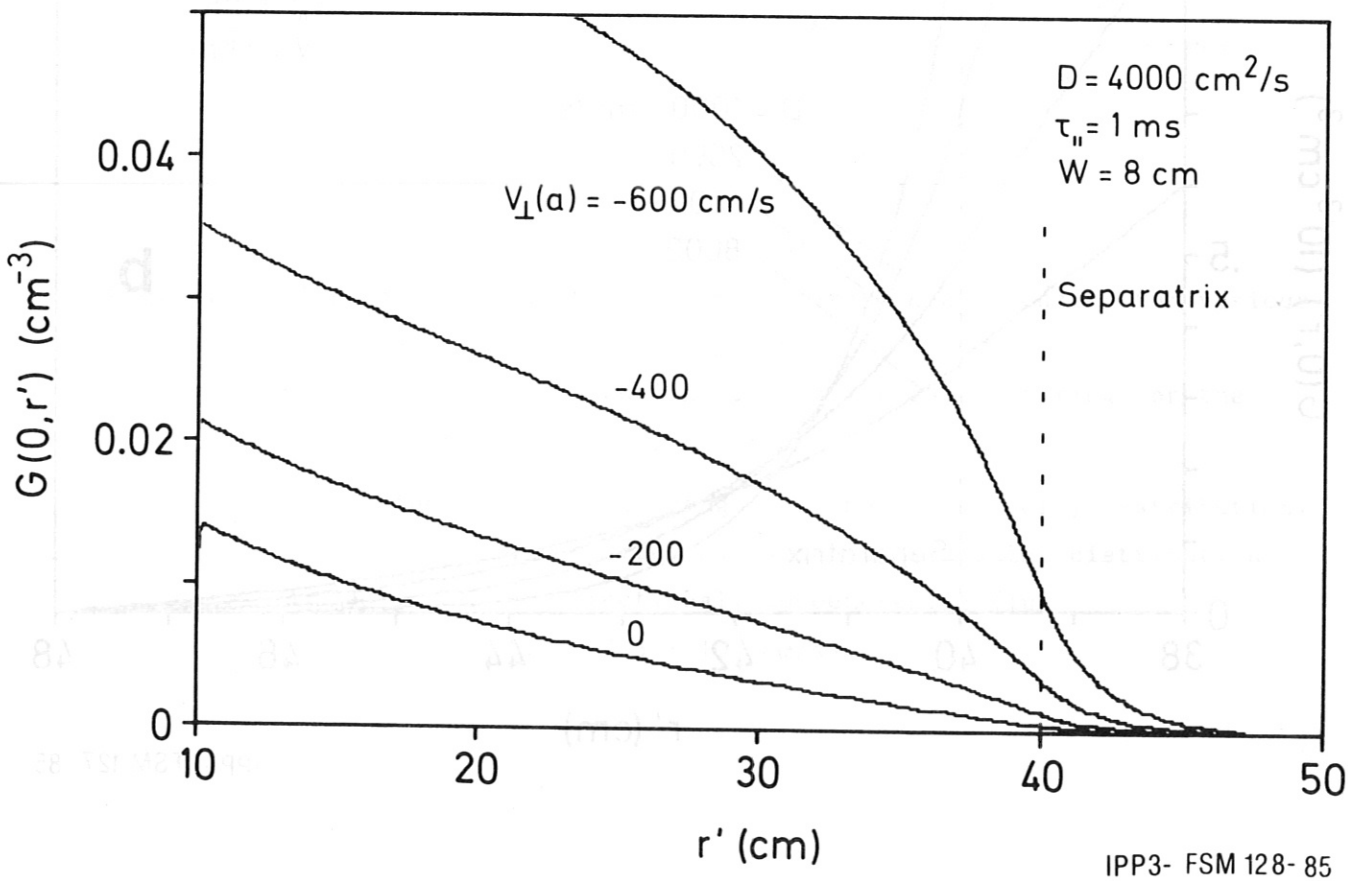

Fig. 2: Central impurity density G(0,r') as a function of source radius r' with the inward drift velocity $v_{\perp a}$ as a parameter ($v_\perp = v_{\perp a}$ r/a, Γ_o = 1 cm^{-2} s^{-1}).

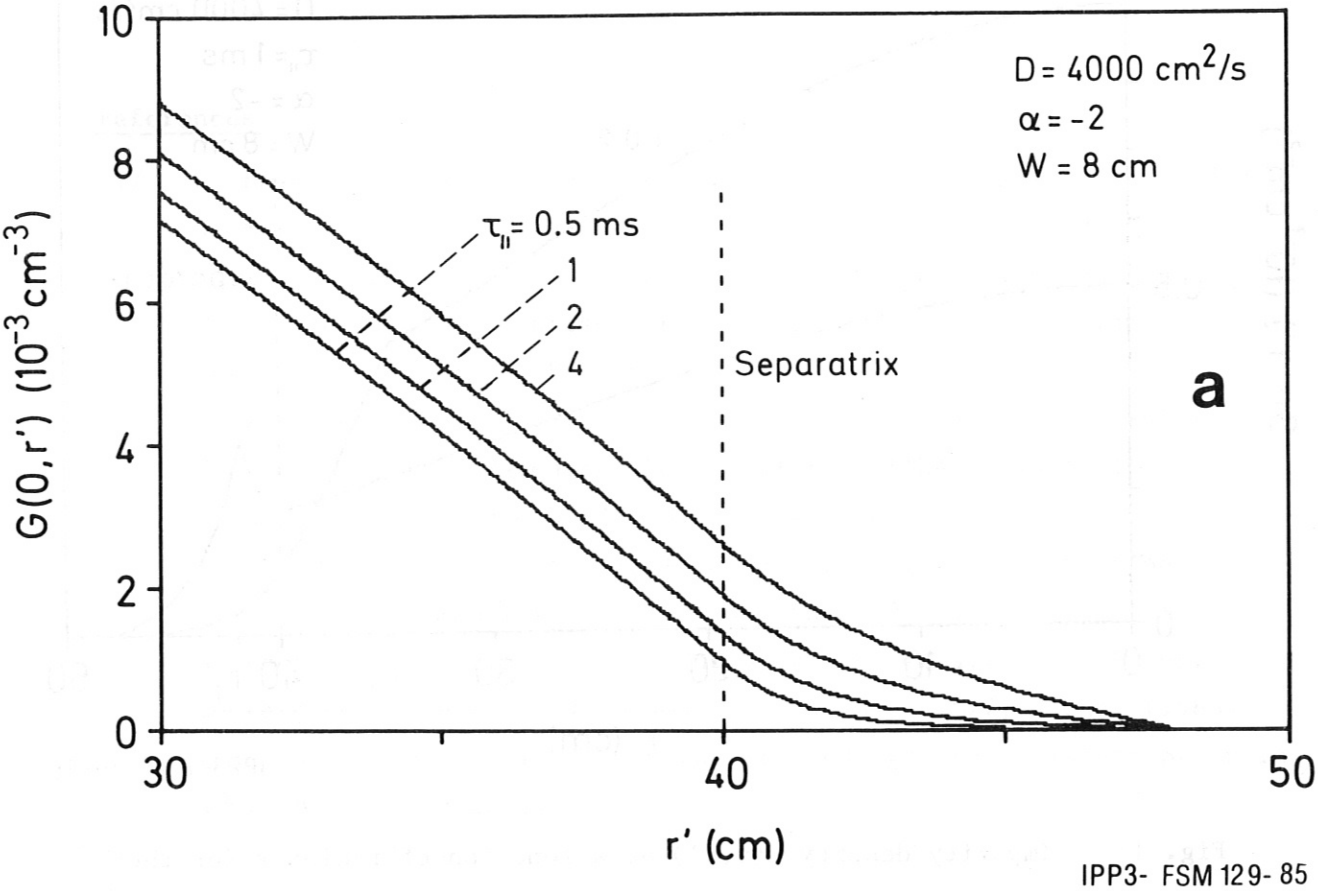

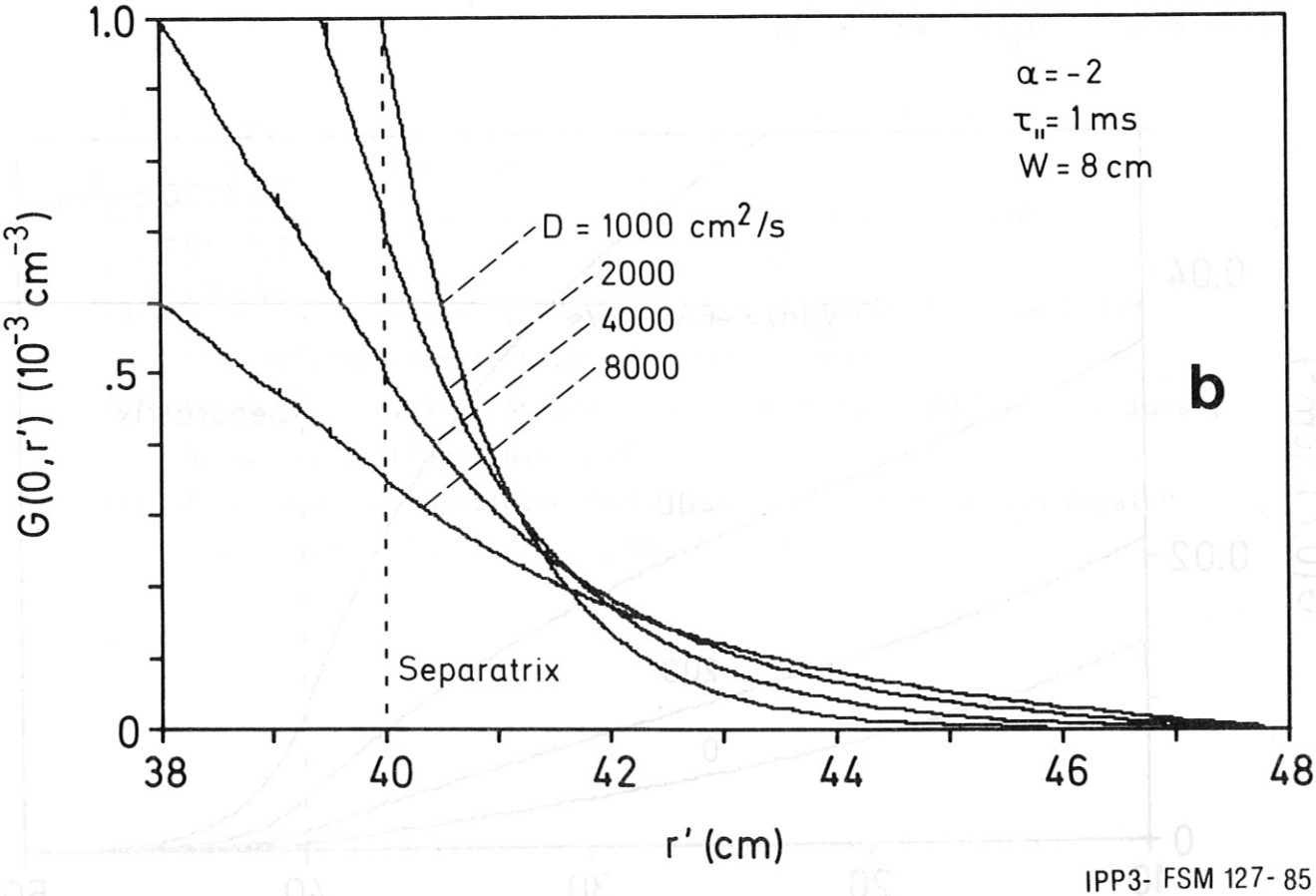

Fig. 3: Central impurity density vs. source radius ($\Gamma_o = 1\ cm^{-2}s^{-1}$) with the parameters $\tau_{\parallel}$ (3a) and D (3b).

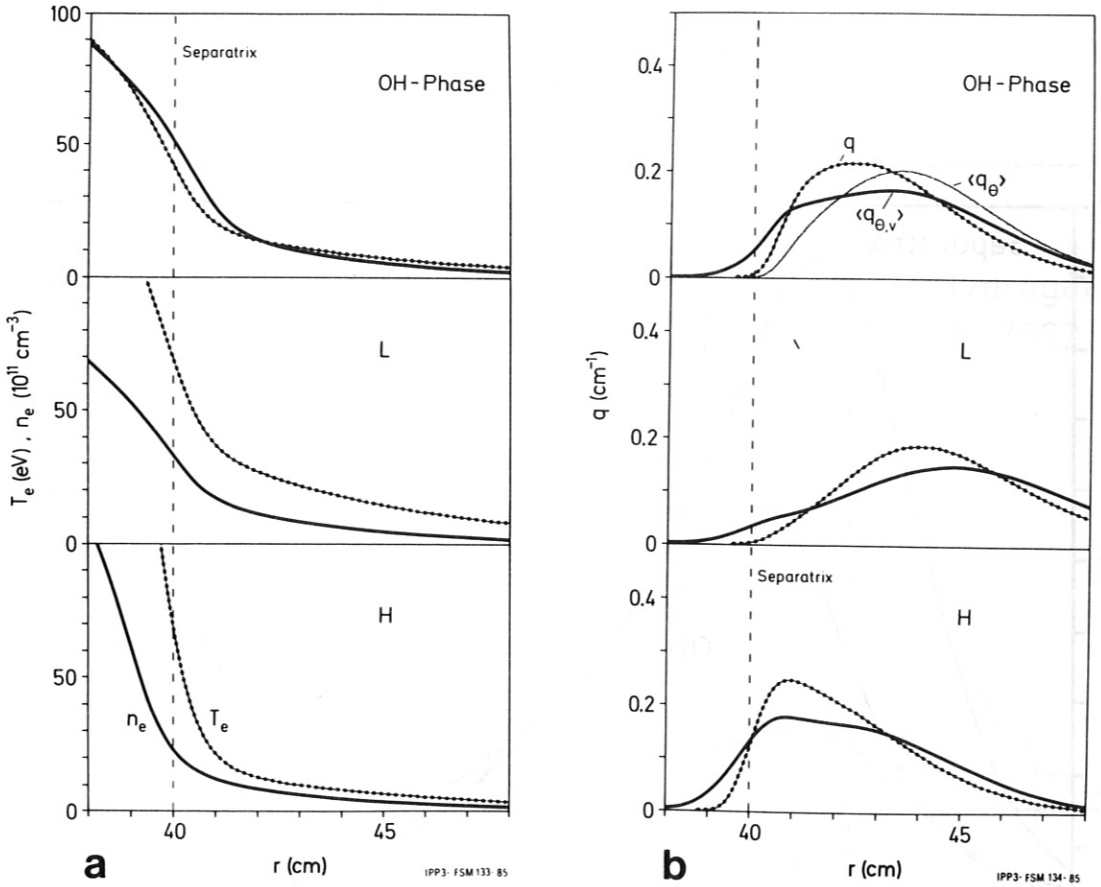

Fig. 4: a) Edge profiles of electron temperature and density for various discharge conditions in ASDEX.

b) Ion source distributions in case of Fe-sputtering for the profiles shown in a).

Solid lines: after averaging over the Fe^o-velocity distribution.

$\langle q_\theta \rangle$: after averaging over angular distribution

Dotted lines: unidirectional, monoenergetic flux

($v_o = 2.3 \cdot 10^5$ cm/s).

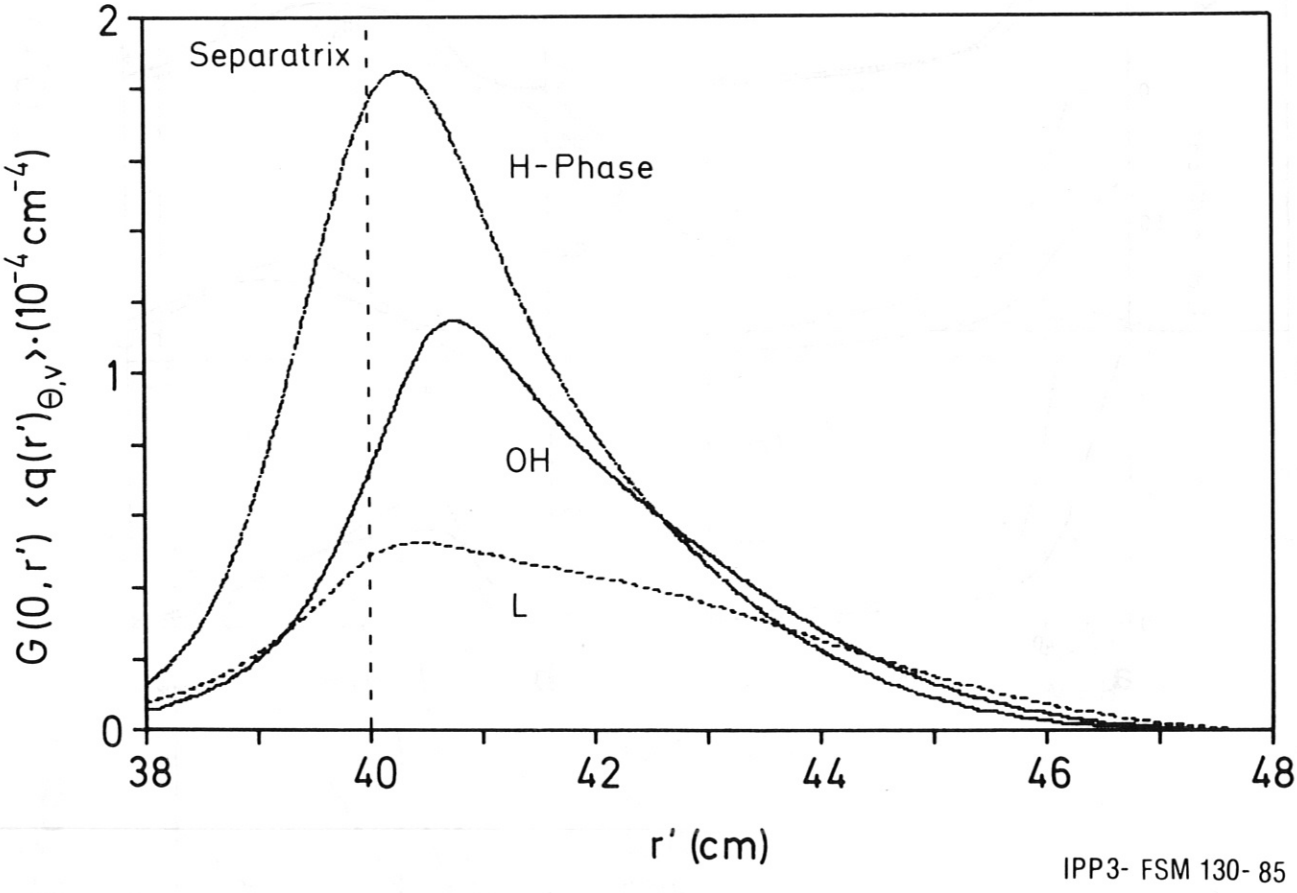

Fig. 5: The integrand of eq. (25a) for the three cases shown in Fig. 4. The area under the curves is representative for the central impurity density $n^{+}(0)$.

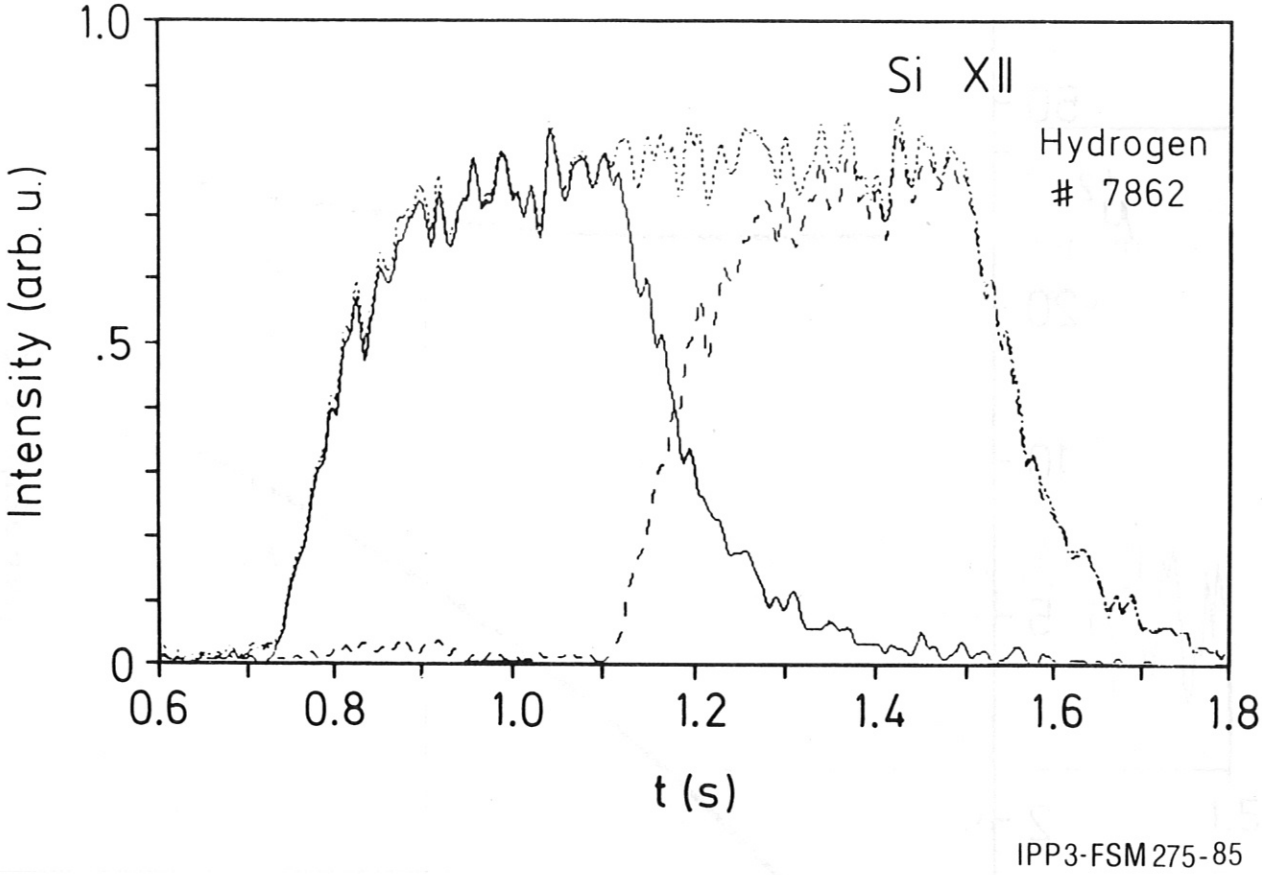

Fig. 6: Measurement of the Si XII line intensity in case of continuous puffing of SiH_4 in ASDEX for the time interval $0.715 \leq t \leq 1.115$ s (solid line). Also shown: Intensity trace shifted by $\Delta t = 0.4$ s (dashed) and the sum of shifted and unshifted signals (dotted). The constancy of the dotted line during the interval 1.1 - 1.5 s documents the complementarity of impurity build-up and decay.

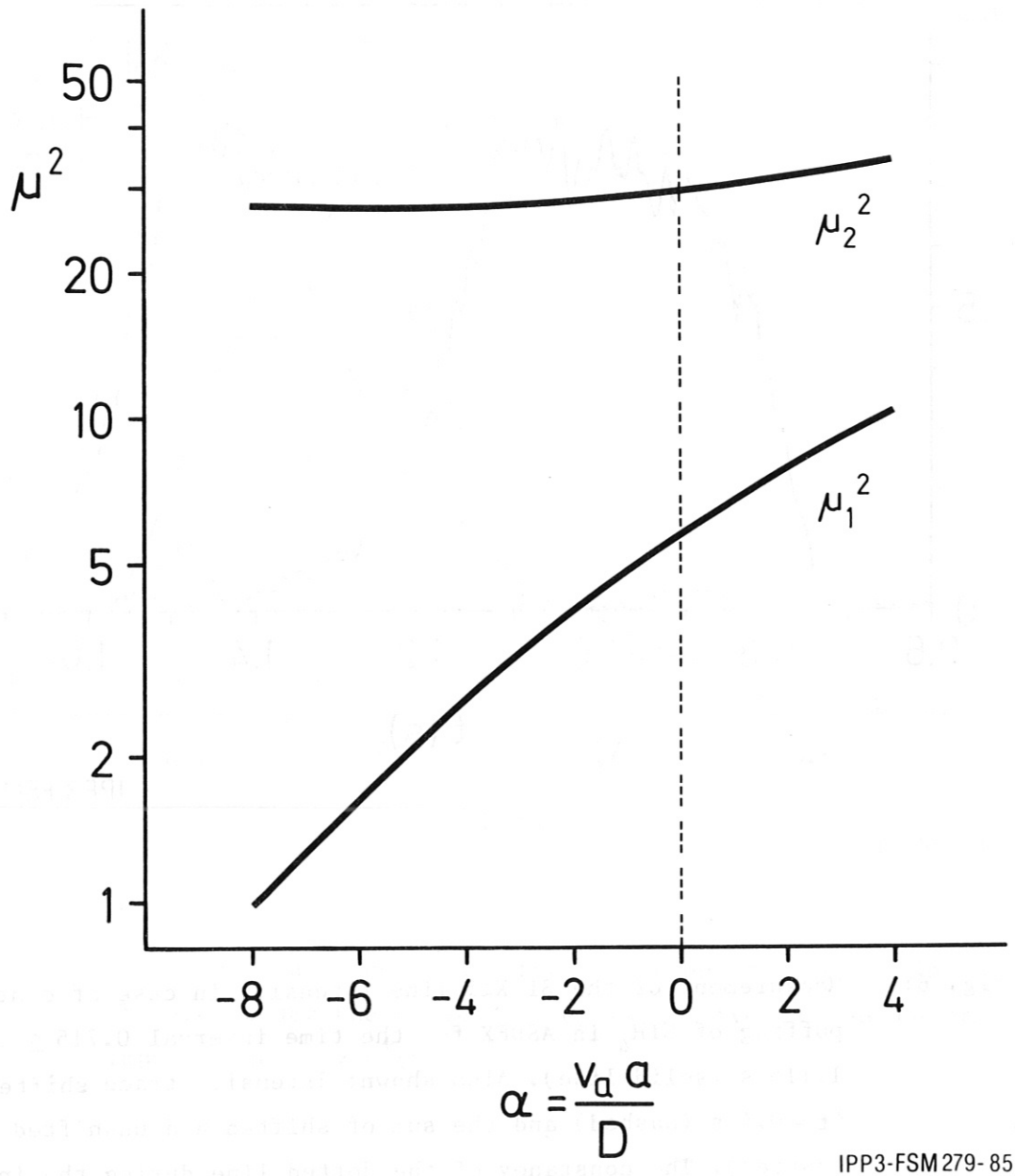

Fig. 7: The two lowest eigenvalues μ_1^2 and μ_2^2 vs. drift parameter α according to eq. (58 b).

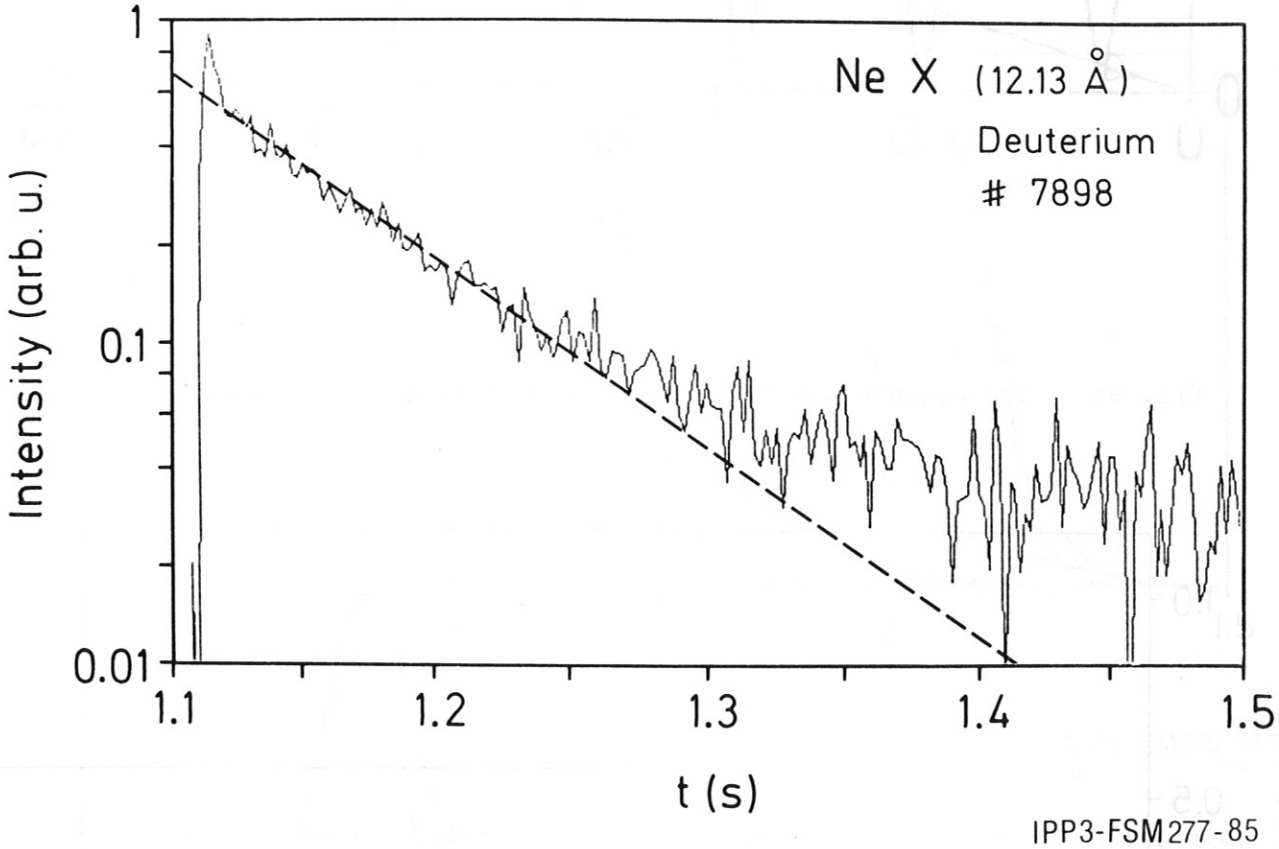

Fig. 8: Log-plot of the measured intensity of Ne X vs. time. The neon was injected into ASDEX by means of a doped pellet. The time constant τ_1 determined from the dashed line amounts to 75 ms.

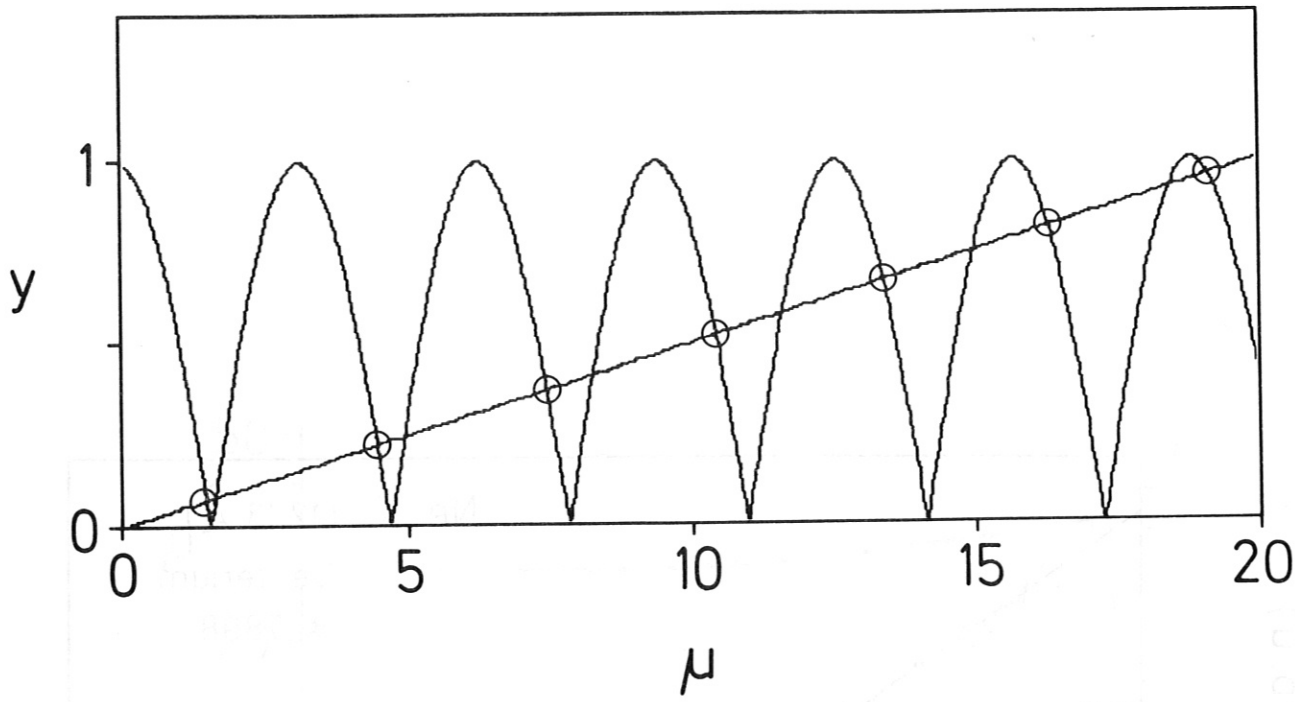

Fig. 9: The eigenvalues μ_n (circles) according to eq. (70 b).

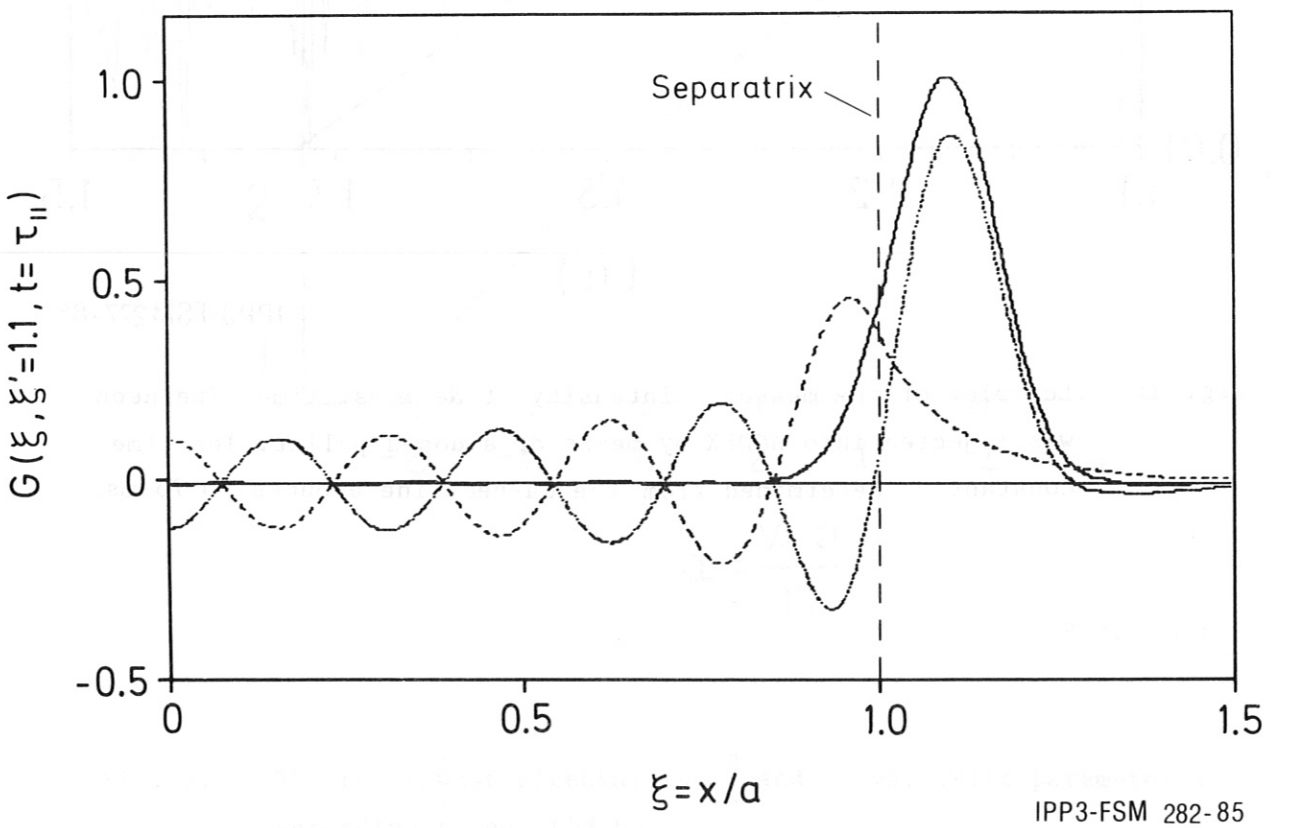

Fig. 10: Green's function $G(\xi,\xi',t)$ according to eq. (72) plotted versus ξ (solid line) for $t = \tau_{II}$ = 1 ms and ξ' = 1.1. The partial contributions of the discrete (dashed) and the continuum spectrum (dotted) are also shown.

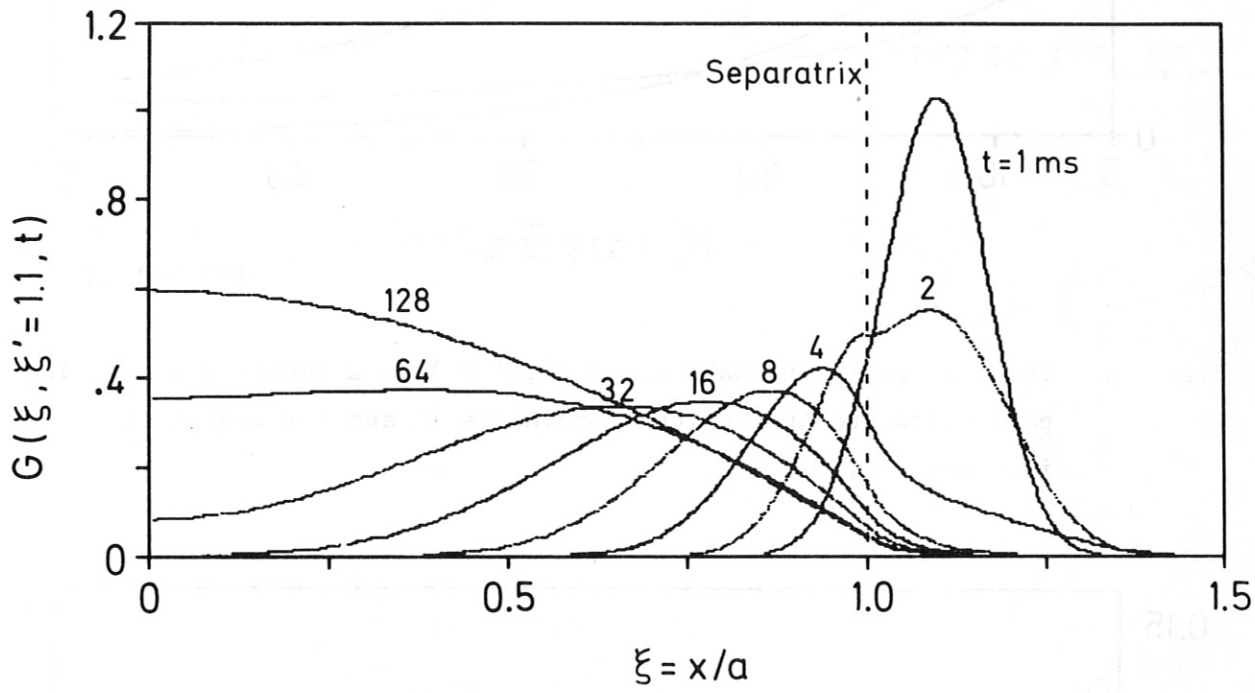

Fig. 11: Propagation and decay of an impurity pulse vs. ξ with the time as a parameter. The amplitudes are magnified by the numbers attached to the curves. The pulse originates as a δ-function in the scrape-off at ξ = 1.1.

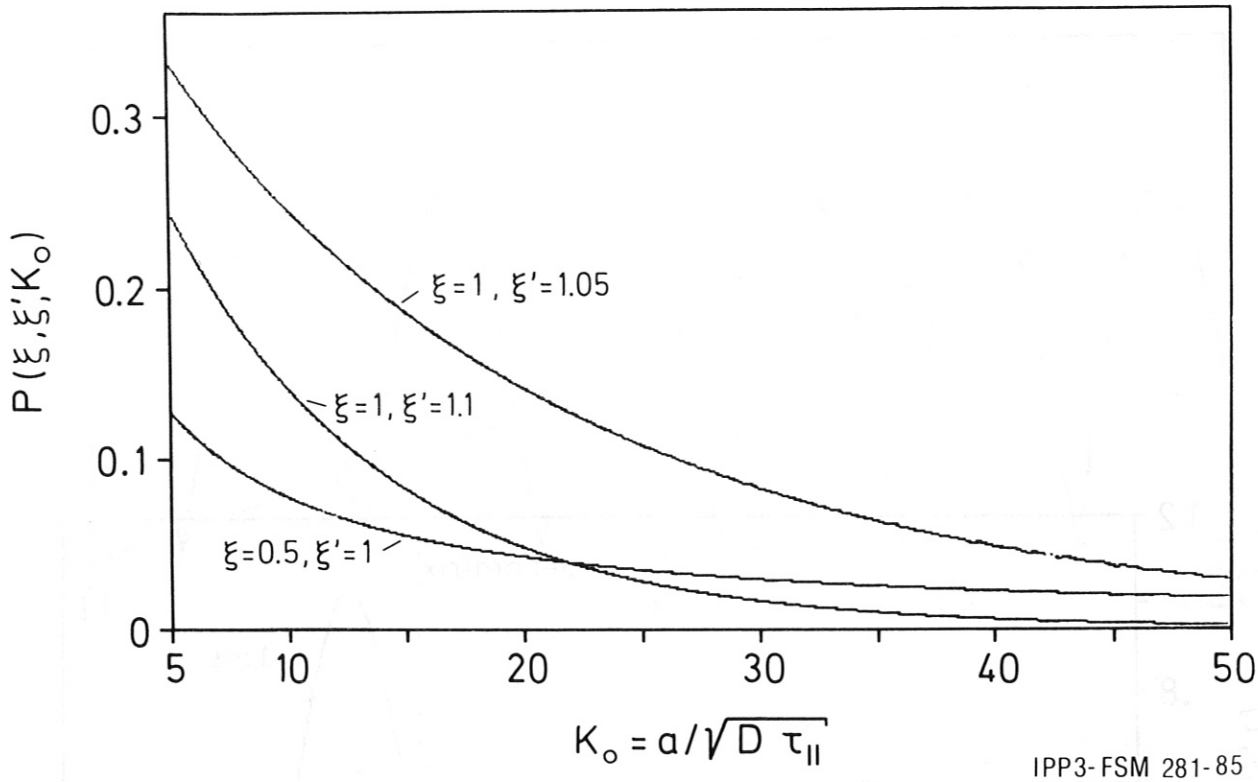

Fig. 12: The penetration probability $P(\xi,\xi',K_o)$ as a function of K_o. The parameters are the source coordinates ξ' and the region of interest $[-\xi,\xi]$.

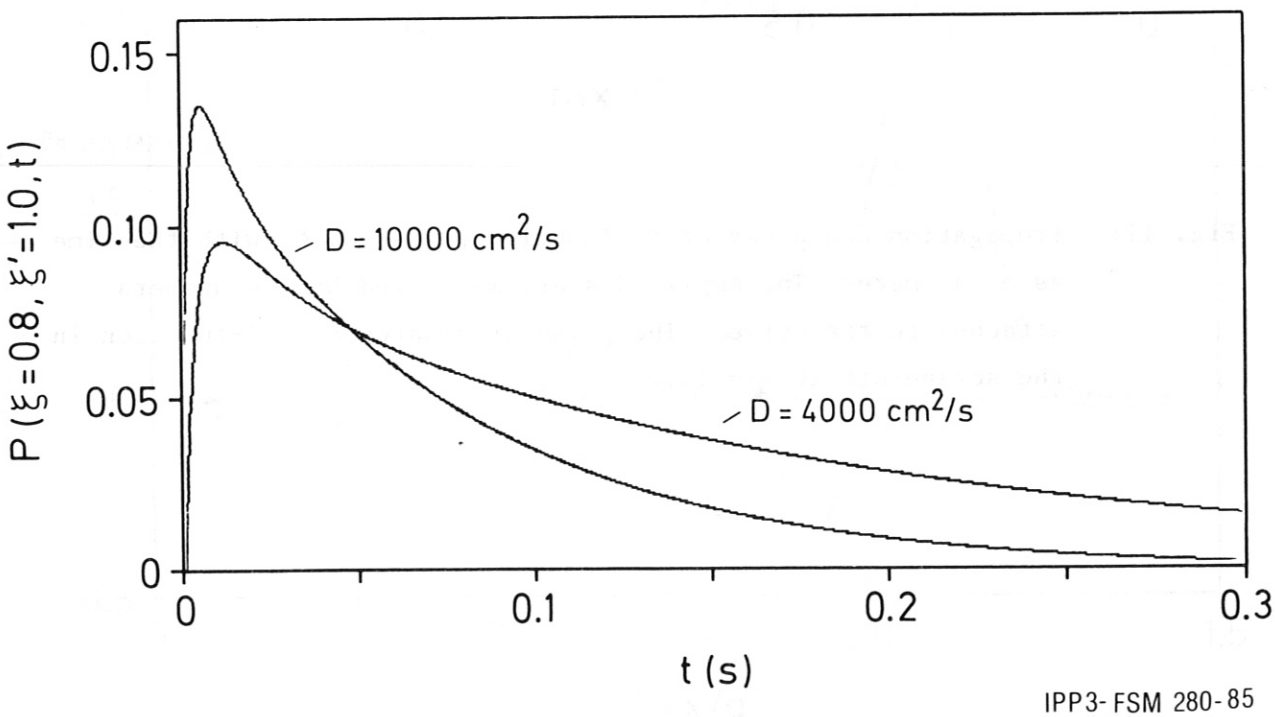

Fig. 13: The residence probability $P(\xi,\xi',t)$ as a function of time for two values of the diffusion coefficient. The source coordinate is $\xi' = 1$, the region of interest $|\xi| \leq 0.8$.